# Magnetic petrology of the Devonian Achala Batholith, Argentina: titanohaematite as an indicator of highly oxidized magma during crystallization and cooling

S. E. Geuna,[1] S. A. McEnroe,[2] P. Robinson[2] and L. D. Escosteguy[3]

[1]*Consejo Nacional de Investigaciones Científicas y Técnicas (CONICET) Instituto de Geofísica 'Daniel Valencio' (INGEODAV), Facultad de Ciencias Exactas y Naturales, Ciudad Universitaria, Pabellón 2, Universidad de Buenos Aires, Argentina. E-mail: geuna@gl.fcen.uba.ar*
[2]*Geological Survey of Norway, Trondheim, Norway*
[3]*Servicio Geológico Minero Argentino (SEGEMAR), Buenos Aires, Argentina*

## SUMMARY

Devonian magmatism in the Eastern Sierras Pampeanas (Córdoba, Argentina) is represented by elliptical, porphyritic, batholithic, late- to post-orogenic monzogranites emplaced in a metamorphic–plutonic basement. Two groups of Devonian granitoids are distinguished: (1) metaaluminous to weakly peraluminous, hornblende-biotite bearing granitoids, and (2) peraluminous, biotite-(muscovite) bearing granitoids. Groups 1 and 2 are characterized by accessory phases of sphene-magnetite with high susceptibility, and ilmenite-(monazite-uraninite) with low susceptibility, respectively. The magnetic assemblage of the Group 2 Achala Batholith, predominantly paramagnetic, is the subject of this paper.

Forty-three sites were sampled in the Achala monzogranite. Overall, it is weakly magnetic, with a mean magnetic susceptibility of $1.5 \times 10^{-4}$ SI. Twenty-one sites showed titanohaematite as the magnetic carrier of a stable remanence. The titanohaematite is an accessory mineral and contains exsolved disc-shaped intergrowths of ilmenite.

The weak magnetism of Achala monzogranite facies contrasts with the magnetic character of other Devonian porphyritic, batholithic monzogranites in the region. The virtual absence of magnetite, together with the presence of exsolved titanohaematite and Mn-ilmenite indicate crystallization and cooling under more oxidizing conditions. Oxidizing conditions continued into the subsolidus, causing late-stage reactions of ilmenite host grains to ilmenite + rutile + haematite, and titanohaematite to ilmenite-poorer haematite + rutile. These reactions resulted in low susceptibility values and a strong reduction of natural remanent magnetization (NRM) intensities.

Thermal demagnetization, up to 620–640 °C, isolated steeply dipping, dual-polarity remanence directions. The coincidence of the Achala paleomagnetic pole with the 380–360 Myr segment of the Gondwana Apparent Polar Wander Path and the U-Pb zircon age implies that the remanence was acquired soon after emplacement.

**Key words:** Magnetic Mineralogy and Petrology; Rock and mineral magnetism; Physics and chemistry of magma bodies; South America.

## INTRODUCTION

Magnetic properties of rocks reflect the partitioning of iron between strongly magnetic oxides (and/or sulphides) and weakly magnetic phases such as silicates. This partitioning is controlled by chemical composition, oxidation ratio of the iron and petrogenetic conditions. This is the basis of magnetic petrology, a discipline that integrates rock magnetism and conventional petrology to characterize the composition, abundance, microstructure and paragenesis of magnetic minerals, to define the processes that create, alter and destroy magnetic minerals in rocks (Clark 1997, 1999).

Rock-magnetic procedures detect trace amounts of magnetic material in rocks. The magnetic susceptibility (MS) of a rock depends of whether its magnetic properties are dominated by paramagnetic or ferromagnetic minerals and their abundances. A rock is considered paramagnetic overall, when it has a MS low enough to rule out the presence of ferromagnetic minerals (MS $< 3$–$15 \times 10^{-4}$ SI). The influence of magnetite in MS comes to dominate the magnetic properties of the rock (which becomes ferromagnetic), when it is present in abundances as low as 0.02 volume percent. A rock is described as ferromagnetic when MS is higher than $1$–$5 \times 10^{-3}$ SI (for variations in the limits see Rochette 1987; Tarling & Hrouda 1993; Clark 1999).

925

Iron-titanium oxide mineralogy was the basis for the descriptive classification of calc-alkaline granitoids, proposed by Ishihara (1981), into a magnetite-series and an ilmenite-series. This classification can be directly related to magnetic properties, because magnetite-series granitoids are ferromagnetic, usually containing 2 volume per cent oxides, whereas ilmenite-series are generally paramagnetic and very low in opaque oxide content. The two series are considered to have resulted from the prevalence of different oxygen fugacites during genesis, where the magnetite-series are significantly more oxidized than ilmenite-series granitoids. S-type (i.e. derived from melting of meta-sedimentary rocks) granites, as defined for the Lachlan Fold Belt in Australia (Chappell & White 1974), are a classic example of reduced ilmenite-series granitoids, whereas I-type (i.e. derived from melting of an igneous source material) can belong either to ilmenite- or magnetite-series, but are usually oxidized more than S-type granitoids (e.g. Ishihara 1981; Whalen & Chappell 1988).

Paleomagnetic and rock-magnetic studies are presented here on the Achala Batholith, a post-kinematic Devonian granitic complex, intruded into Proterozoic basement, forming the Eastern Sierras Pampeanas of Argentina. Although low MS values point to classify the components of the Achala Batholith as paramagnetic, we have found that its opaque mineralogy is not typical for the classic reduced calc-alkaline granitoids. It is characterized by the presence of up to 1 volume percent opaque minerals, dominated by the ilmenite-haematite solid solution instead of pure ilmenite or magnetite. In this paper, based on paleomagnetic and rock-magnetic study, we discuss the implications of the presence of coexisting titanohaematite and Mn-bearing ilmenite in the Achala Batholith because they point to the prevalence of oxidizing conditions during magmatic crystallization and cooling.

# GEOLOGICAL BACKGROUND, OXIDIZED VERSUS REDUCED GRANITES

## Eastern Sierras Pampeanas geological setting

The Eastern Sierras Pampeanas are north-trending, west-verging, fault-bounded basement uplifts in Central Argentina, consisting mainly of Precambrian age amphibolite- to granulite-facies metamorphic and plutonic rocks. The basement is intruded by a number of granitoid types, representing igneous activity in the Early Paleozoic cratonic margin of Gondwana.

The Eastern Sierras Pampeanas granitoids have been classified, according to their temporal relationship with the main Ordovician deformation episode, into pre-, syn and late to post-orogenic (Sato *et al.* 2003). The late- to post-orogenic (LPO) magmatism is the most abundant, being represented by many subcircular, discordant, high-K plutons (Fig. 1a). Geochemically, these plutons plot as collisional or intraplate granites, and show high large ion lithophile and high field strength elements (Y-Nb) (Rapela *et al.* 1990).

The LPO granites reach batholithic dimensions, in complexes emplaced and cooled quickly, in high-level crust (depths less than 7.5 km, de Patiño & Patiño Douce 1987; Pinotti *et al.* 2002). Porphyritic facies with microcline megacrysts are dominant. They are locally surrounded by contact metamorphic aureoles. Compositionally, they include calc-alkaline to alkaline granites and are metaluminous to peraluminous. Monzogranites-granites are more abundant, with granodiorites, leucogranites and tonalites subordinate. Mafic enclaves, late aplite-pegmatite and lamprophyre dykes are also com-

mon. U-Pb crystallization ages range from 393 ± 5 (Stuart-Smith *et al.* 1999) to 368 ± 2 Myr (Dorais *et al.* 1997). The LPO granites have been attributed to late stages of the Ordovician Famatinian Orogeny (Rapela *et al.* 1990; Sato *et al.* 2003) or to a separate Devonian magmatic cycle, the 'Achalian' (Sims *et al.* 1998; Stuart-Smith *et al.* 1999). These represent the product of intracontinental crust, partially molten due to a change in the thermal regime during regional uplift (Otamendi *et al.* 2002), possibly as a result of the accretion of the Precordillera terrane (Rapela *et al.* 1998) or Chilenia (Stuart-Smith *et al.* 1999) to the Gondwana margin.

Two groups can be distinguished in LPO granites. The first is composed of metaaluminous to weakly peraluminous, hornblende-biotite-bearing granitoids. The second is formed by peraluminous, biotite-(muscovite)-bearing granitoids. The two groups are characterized, respectively, by sphene-magnetite and ilmenite-(monacite-uraninite) as accessory phases, resulting in distinctive magnetic properties (Geuna *et al.* 2008a). The Renca and La Totora Batholiths (Fig. 1a), described by López de Luchi *et al.* (2002, 2004), are examples of ferromagnetic hornblende-bearing granitoids. Magnetic properties from the second group, Achala Batholith, are dominantly paramagnetic (i.e. very low susceptibility) and are presented in this paper.

## The oxidation state of granites

Blevin (1994) has shown that ferric/ferrous iron ratios in granitoid rocks are highly correlated with oxygen fugacity as calculated from the chemical composition. The redox states of granitic magmas are essentially intrinsic in nature and may reflect the redox states of magma source regions.

The oxidation state can also be established by using petrographic and mineralogical criteria, whole rock $Fe_2O_3/FeO$ ratios, and geophysical methods. Blevin (2003), using correlation of these parameters, developed a classification scheme based on whole rock $Fe_2O_3/FeO$ and FeO,* (total Fe). Rocks belonging to each of these divisions can be characterized by distinctive petrographic and mineralogical features. Strongly oxidized rocks are typically represented by igneous suites associated with economic porphyry Cu–Au systems and have abundant magnetite, sphene and high-Mg biotite. There is a general trend to lower relative oxidation state in granites from arc settings, through continental margin settings, to those of continental interiors. S-types are usually reduced (Blevin & Chappell 1995). Many S-type granites come from partial melting of graphitic schists (black shale), but haematite shales are also a possible source.

A correlation exists between MS, $SiO_2$ and $Fe_2O_3/FeO$, with MS values used to distinguish between ilmenite- and magnetite-series granites, which in turn, can be interpreted as representing reduced or oxidized magmas, respectively.

However, exceptions exist. Very oxidized rocks usually contain haematite, rather than magnetite, and are weakly magnetic, like reduced ilmenite-series rocks (Clark 1999). Very felsic granitoids ($SiO_2 > 72$ wt per cent) have iron contents too low to crystallize significant magnetite, irrespective of oxidation state. More importantly, granites with evidence of alteration of magnetite show little correlation between susceptibility, $SiO_2$ and $Fe_2O_3/FeO$, indicating that the processes of magnetite alteration are not systematically related to granitoid composition (Clark 1999).

Oxidation state of classic I- and S-type granitoids of the Lachlan Fold Belt are plotted on Fig. 2(a). The figure shows the difference in oxidation ratio for both series, but also the wide compositional
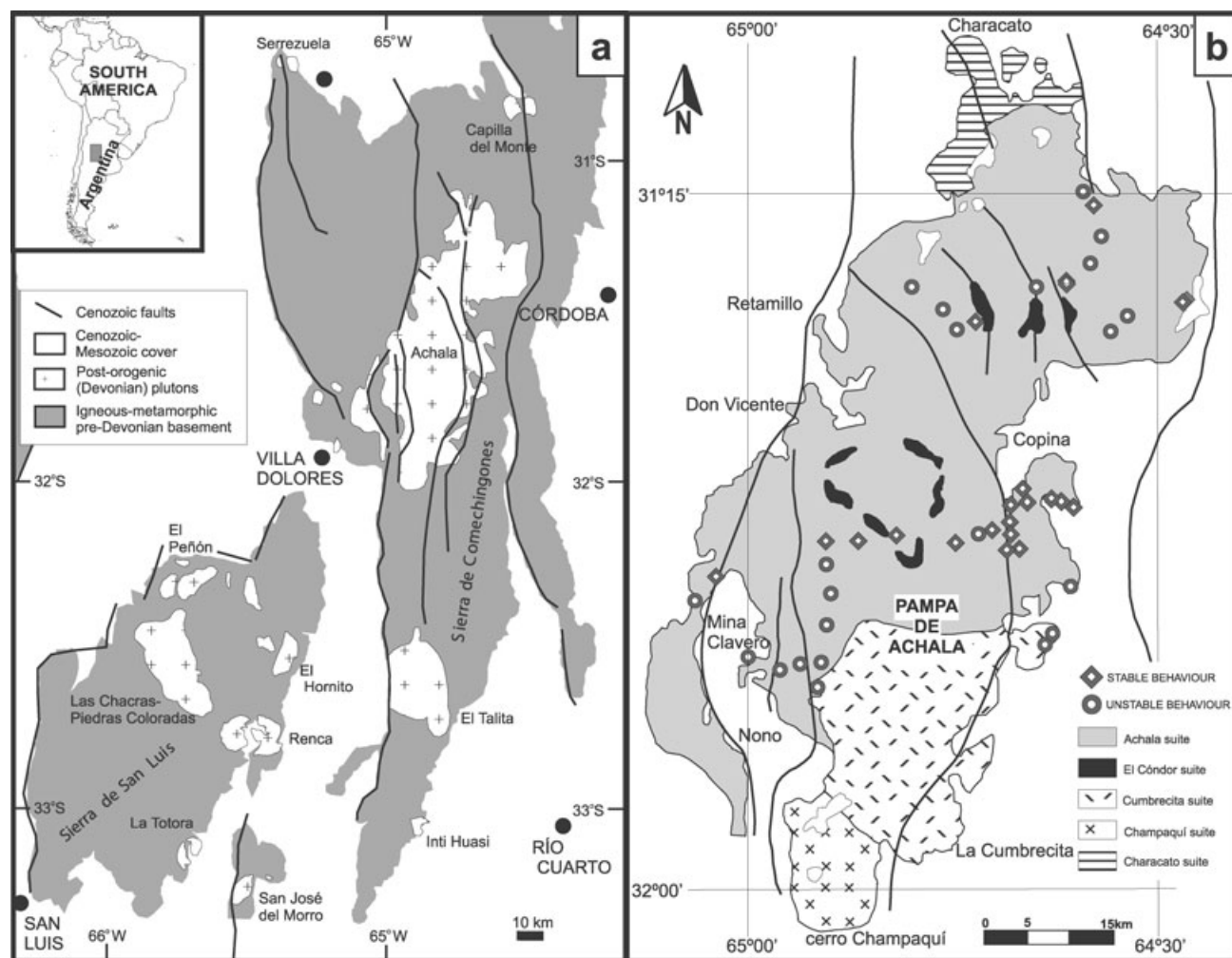
**Figure 1.** (a) Geological map of Eastern Sierras Pampeanas (Argentina) showing the location of late to post-orogenic (LPO) Devonian granitoids. Modified from Pinotti *et al.* (2002) and Sato *et al.* (2003). (b) Location of the sampling sites on Achala Batholith (geology modified from Demange *et al.* 1996).

variation of I-type granitoids, as opposed to the restricted composition of S-type series (Chappell & White 1974). Fig. 2(b) shows that, although oxidation ratios for Japanese magnetite-series granitoids approximately coincide with that for I-type field in Fig. 2(a), ilmenite-series samples do not strictly correspond to the S-type field. Instead, ilmenite-series show wide compositional variation, implying that, as shown by Whalen and Chappell (1988), this series correlates to S-type plus reduced I-type granitoids.

The oxidation state of LPO granites from Eastern Sierras Pampeanas is plotted in Fig. 2(c). Very felsic granites usually have exaggerated ratios or are susceptible to alteration effects, particularly when $FeO^* < 1$ wt percent (Blevin 2003). The $Fe_2O_3/FeO$ ratios for rocks with $FeO^* < 2$ wt percent, has been considered not representative of the actual oxidation state by Blevin (2005); in these cases, reference to related samples with higher $FeO^*$ contents has been suggested. It seems clear that the low $FeO^*$ content is related with high dispersion in $Fe^{3+}/Fe^{2+}$, for both paramagnetic Achala Suite and ferromagnetic Renca equigranular monzogranites. However, when we compare the values for rocks with higher $FeO^*$ contents, like the El Cóndor Suite against Renca porphyroid monzogranites, they both follow a discrete trend outside the reduced field typical of ilmenite-series granites. Remarkably, the El Cóndor

Suite of Achala plots in a more oxidized region in Fig. 2(c) than the magnetite-bearing Renca porphyroid granite field.

## Opaque petrography of oxidized and reduced granites

Though oxide compositions have the ability to re-equilibrate externally during cooling, and oxide compositions alone do not perfectly predict oxidation conditions in slowly cooled rocks (e.g. Czamanske *et al.* 1981; Frost & Lindsley 1991), some features could constitute reasonable indicators.

Both magnetite and ilmenite are generally present in magnetite-series granites, but magnetite constitutes more than 90 per cent of the opaque oxides. On the other hand, ilmenite-series granites are very low in opaque oxide content, usually as plates of ilmenite, mainly in ferromagnesian silicates (Ishihara 1981). Czamanske *et al.* (1981) found that ilmenite-series granites have ilmenite with low contents of $Fe_2O_3$ ($Hem_3$ is representative), whereas magnetite-series have ilmenites with representative composition $Hem_{15}$.

In an attempt to correlate I- and S-type granites with magnetite- and ilmenite-series, Whalen & Chappell (1988) characterized the opaque mineral assemblages in Lachlan Fold Belt granites.
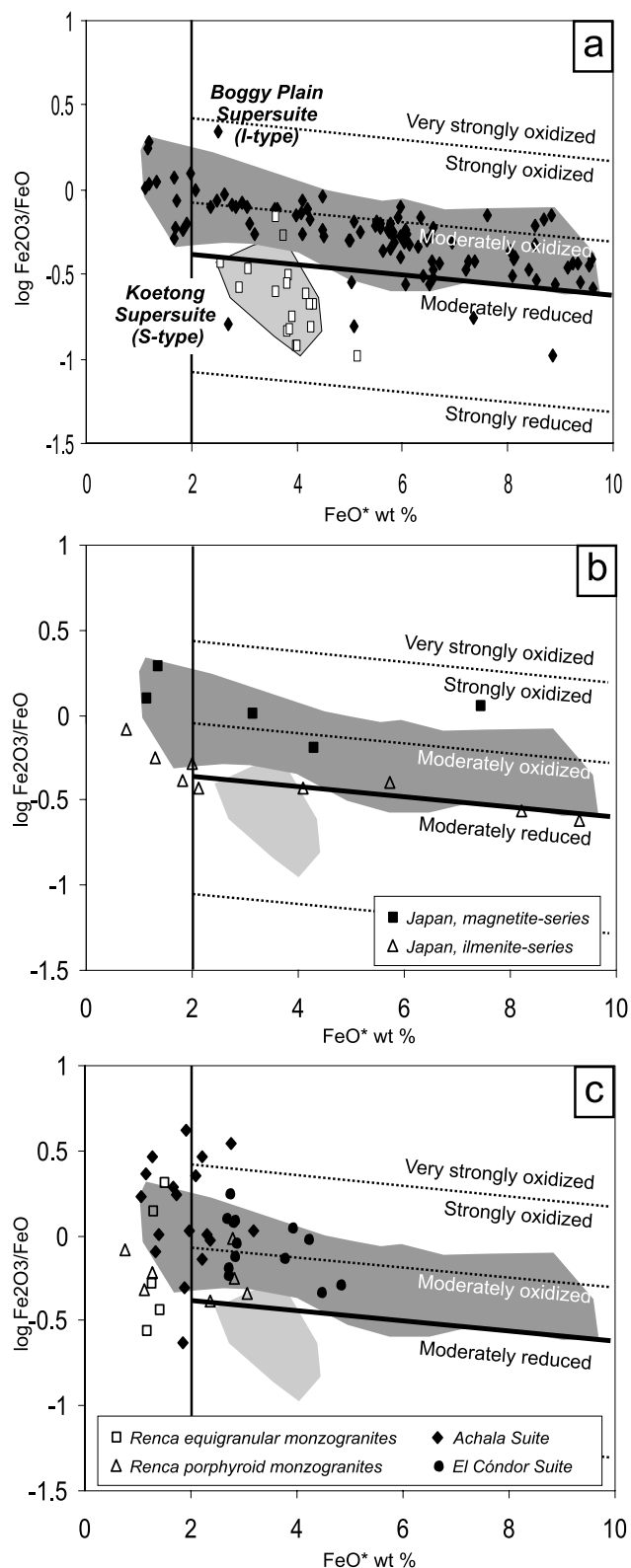
**Figure 2.** A plot of $Fe_2O_3/FeO$ versus total Fe as FeO (wt percent) showing the fields for strongly reduced, reduced, oxidized and strongly oxidized, from Blevin (2003). The vertical boundary at 2 wt percent FeO* has been introduced by Blevin (2005) to remark that $Fe_2O_3/FeO$ for rocks with lower FeO* contents are not representative of their actual oxidation states. (a) S- and I-type granites from Lachlan Fold Belt; data from Geoscience Australia Ozchem database. (b) ilmenite- and magnetite-series granites from Japan, data from Czamanske *et al.* (1981). (c) Achala and Renca batholiths, data from de Patiño (1989) and López de Luchi (1986), respectively.

They found that magnetite + ilmenite + minor sulfide (pyrite > chalcopyrite > pyrrhotite) generally characterize I-type granites, whereas ilmenite + sulfide (pyrrhotite > pyrite > chalcopyrite) are usually present in S-type granites. They concluded on the basis of rock chemistry, opaque mineral assemblages and mafic mineral chemistry that most Lachlan S-type granites formed at lower $fO_2$ conditions than most Lachlan I-type granites. For example, they only found haematite exsolution lamellae in ilmenite parallel to {0001} in some I-type granites. In S-type granites, ilmenite was generally fresh, but if altered, it was to rutile with no haematite. Ilmenite in the S-type suites contain little or no $Fe_2O_3$ and has relatively low $MnTiO_3$ and high $FeTiO_3$ contents, whereas in the I-type suites, average $MnTiO_3$ and $Fe_2O_3$ contents are higher.

## THE EASTERN SIERRAS PAMPEANAS LATE- TO POST-OROGENIC GRANITOIDS

### Ferromagnetic granitoids: the Renca batholith

The Renca Batholith is an elliptical zoned pluton comprising two main facies: an external grey to slightly pinkish porphyritic biotite-hornblende granodiorite/monzogranite (Unit 1) and a central pink to grey equigranular biotite–muscovite monzo/leucomonzogranite (Unit 2; López de Luchi *et al.* 2002). U/Pb zircon yielded a crystallization age of 393 ± 5 Myr (Stuart-Smith *et al.* 1999) whereas K/Ar mineral ages on biotite indicated 382 ± 17 Myr.

Decompressional melting of an enriched mantle, together with melting of an already depleted lower crust that has received a thermal input from the metasomatized mantle, during orogenic collapse, has been proposed for the batholith (López de Luchi 1996).

Bulk MS measurements show a bimodal distribution with Unit 1 ferromagnetic, with a mean MS of $7 \times 10^{-3}$ SI, and Unit 2, paramagnetic, with a mean MS of $1 \times 10^{-4}$ SI. A similar distribution is observed for the intensity of natural remanent magnetization (NRM).

Preliminary paleomagnetic results indicated the presence of a stable, dual polarity, very steep magnetization in many sites, but these are poorly defined. Microscopic observations of polished sections revealed that Unit 1 is characterized by the presence of multidomain magnetite as scarce large crystals ($>100$ $\mu$m) with incipient martitization along {111} planes, commonly associated with sphene and biotite. Grains of primary titanohaematite with exsolved ilmenite are also observed. Unit 2 shows the same association, but unaltered magnetite is rare, and martitization is nearly complete (López de Luchi *et al.* 2002). The main ferromagnetic mineral in the Renca porphyroid monzogranite is magnetite, appearing as a stable phase throughout the pluton's crystallization history. Bulk susceptibility values are locally lower due to magnetite alteration, which is maximum in Unit 2 (López de Luchi *et al.* 2002).

Magnetite is the dominant magnetic carrier in Las Chacras (Siegesmund *et al.* 2003), La Totora (López de Luchi *et al.* 2004) and El Talita (Pinotti *et al.* 2006) Devonian granitoids (see locations in Fig. 1a).

### Paramagnetic granitoids: Achala Batholith

The Achala Batholith is one of the largest examples of LPO granites; it has an elliptical shape trending N-NE, with a maximum extension of 100 × 50 km (Fig. 1b). Its contacts are regionally sharp and discordant. Based on gravity anomalies measured along

a regional transect the vertical extension is estimated to be about 6 km (Introcaso *et al.* 1987).

Demange *et al.* (1996) distinguished five independent magmatic suites, the Achala suite being the most extensive (Fig. 1b), and suggested that all five suites are nearly coeval but derived from different parental magmatic sources. Overall the batholith is a peraluminous, alkali-calcic granitoid developed at great distance from the subduction margin in the last stage of magmatic arc evolution (Rapela *et al.* 1990).

The most abundant rock type in the batholith is a high-K, coarse-grained to porphyritic monzogranite, with variable amounts of K-feldspar megacrysts. Lira & Kirschbaum (1990) described the Achala granitoids as formed of quartz, microcline, plagioclase, biotite and muscovite. Accessory phases are fluorapatite, zircon, iron oxides, chlorite, rutile and kaolinite. Ratios of biotite to muscovite are variable, with total mica about 10 per cent. The biotite is pleochroic from dark brown to yellowish brown or light yellow and contains variable amounts of Ti and U. Both primary and secondary muscovite is present. Uraniferous minerals include uraninite, pitchblende, gummite, autunite-metautunite, torbernite-metatorbernite and uranophane (Lira & Kirschbaum 1990).

Deuteric alteration effects include the partial replacement of feldspar and biotite by muscovite accompanied by phengite and iron-titanium oxide (Lira & Kirschbaum 1990). Selvage-style greisenization is widespread, developed around fracture zones due to meteoric water, below 250–350 °C (Lira *et al.* 1996).

The crystallization age of the main facies was determined by Dorais *et al.* (1997) at $368 \pm 2$ Myr, based on analyses of zircons from both the granites and its enclaves. Rb/Sr ages varied from $399 \pm 25$ (Rapela *et al.* 1982) to $333 \pm 33$ Myr (Rapela *et al.* 1991). Rb/Sr ages may indicate resetting due to hydrothermal alteration; in this context, the leaching of the alkalis may be responsible for the peraluminous character of the batholith. The alteration is late-magmatic to deuteric (Demange *et al.* 1996) with the last thermal input in the range 300–400 °C at $336 \pm 3$ Myr (K-Ar muscovite), implying that the batholith cooled from emplacement temperatures quickly (Jordan *et al.* 1989). Rapid cooling, completed in about 30 Myr, is reported for other LPO granites in the area (Siegesmund *et al.* 2003).

After emplacement, the batholith was affected by large dextral wrench faults before the Late Carboniferous and inverse faults related to the Cenozoic Andean cycle (Demange *et al.* 1996), resulting in exposures that are dominantly north-trending, eastward-tilted blocks.

### Sampling and laboratory procedures

Samples were collected from the main porphyritic facies of the Achala suite mainly from fresh exposures at road cuts and quarries because weathering is difficult to avoid elsewhere. One hundred and thirty oriented cylinders (2.5 cm diameter) were collected using a portable, gasoline-powered rock drill at 43 sampling sites, distributed along routes 20 and 28 (Fig. 1b). Samples were oriented using both magnetic and sun compasses.

The samples were cut into specimens of 2.2 cm length. Remanent magnetization was measured using a three-axis 2G DC squid cryogenic magnetometer. Alternating field demagnetization (AF) was carried out to a maximum of 110 mT, using a static 2G600 demagnetizer attached to the magnetometer. Step-wise thermal demagnetization up to 680 °C was performed using either a two-chamber ASC or Schonstedt TSD-1 oven.

At least two specimens from each site were subjected to stepwise demagnetization to examine the coercivity and blocking temperature spectra of the NRM. As a general procedure, AF demagnetization was preceded by the application of heating to 150 °C, to eliminate the effects of modern goethite, whereas thermal demagnetization was preceded by the application of low alternating fields (up to 10–20 mT) to minimize the soft components carried by multidomain magnetite. Bulk MS was measured after each thermal step to monitor possible magnetic mineral changes, by using a MS2W Bartington susceptometer.

Isothermal remanent magnetization (IRM) up to 4 T was applied to selected samples to identify the minerals carrying the magnetization. Hysteresis parameters were determined at room temperature in a maximum field of 1 T, by using a Molspin vibrating sample magnetometer at the Instituto Astronomico e Geofisico, Universidade de Sao Paulo (Brazil). Measurement of low-field thermomagnetic curves were made with a prototype bridge at CSIRO facilities in North Ryde, Australia.

Magnetic behaviour of each specimen was analysed by visual inspection of vector endpoint plots, stereographic projections and intensity demagnetization curves.

Compositional data and images of opaque oxides were collected on a Cameca SX-50 electron microprobe (EMP) at the University of Massachusetts (USA), set at an accelerating potential of 15 keV, a sample current of 15 nA and a beam diameter of $1 \mu$m. Counting times of 20 or 40 s per element were used. Corrections for differential matrix effects were made using the Cameca online PAP correction routine. Analytical precision is estimated at $\pm 0.1$ weight per cent for oxide components present at the 1 weight per cent level. Analytical precision on typical values of 0.5 weight per cent $V_2O_3$ and $Cr_2O_3$ is estimated to be $\pm 0.06$ weight per cent at the 95 per cent confidence level. In addition, there is believed to be a systematic overestimate of $V_2O_3$ in ilmenite of about $+0.1$ weight per cent, caused by Ti $K\beta$ -V $K\alpha$ interference.

Three samples, 2–3b, 22–2b, and 38–1 were examined in polished sections in reflected light and in electron backscatter images, followed by electron probe analyses at University of Massachusetts.

## RESULTS

### Magnetic properties of Achala Batholith

Magnetic susceptibility of the Achala main facies is low, ranging from paramagnetic material $5 \times 10^{-5}$ SI, to a weakly ferromagnetic material, $1.5 \times 10^{-3}$ SI. All samples indicate a magnetite content well below 0.1 per cent volume. The NRM is weak, usually between 0.1 and 5 mA m$^{-1}$, although it can be higher in some sites, up to 100 mA m$^{-1}$ (Fig. 3).

In 22 of the 43 sites the magnetic remanence was unstable. These sites usually had very low NRM intensities (0.1–2 mA m$^{-1}$). Remanence of these samples became erratic after demagnetization to 25 mT or 300 °C. This unstable behaviour corresponds to sites with a high degree of weathering.

For the remaining 21 sites, AF demagnetization was effective only to remove a fraction of the remanence, which varied from 0 per cent (Fig. 4) to 80 per cent (Fig. 5), but was usually less than 25 per cent (Table 1). This fraction was demagnetized with fields as low as 15 mT.

The NRM remaining after 15 mT was unaffected by AF demagnetization, revealing coercive forces greater than 100 mT in stable samples (Figs 4 and 5). Thermal demagnetization resulted in
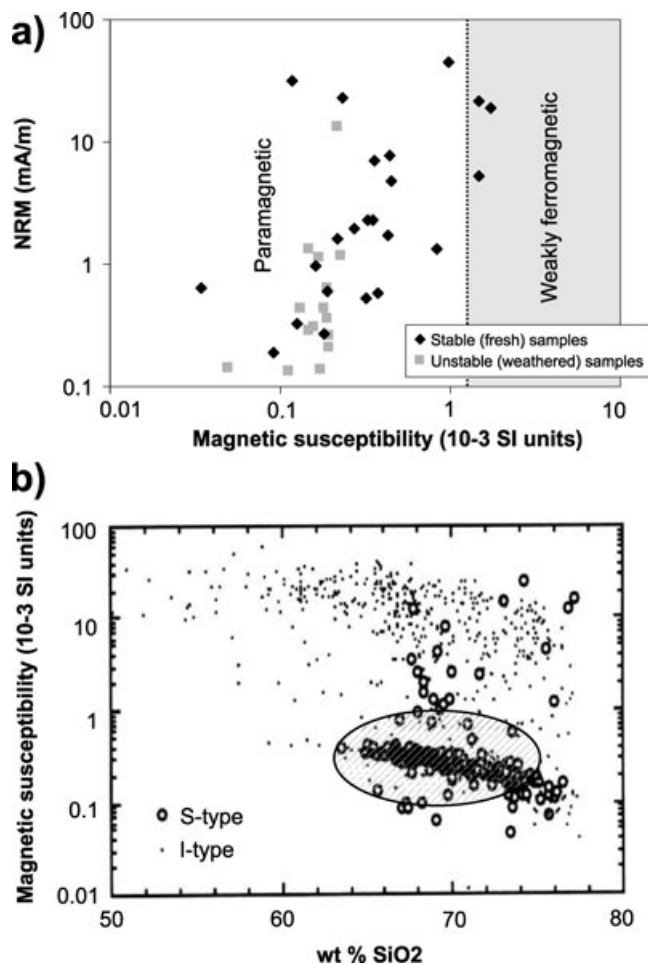
**Figure 3.** (a) Achala Batholith, magnetic susceptibility versus intensity of natural remanent magnetism. Limit between paramagnetic and weakly ferromagnetic fields from Clark (1999). (b) Typical magnetic susceptibility (MS) values for granitoids, from Blevin (1994). Note that S-type granitoids have lower MS than I-type granitoids. The approximate field for Achala samples is shown as a hatched ellipse.

blocky curves with discrete unblocking temperatures of 610–640 °C (Fig. 4a), with some samples showing a second higher unblocking of 670–680 °C (Figs 4b and 5a); despite this variation in unblocking temperatures, only one high-temperature magnetic component was isolated from each sample. When plotted for the stable 21 sites, this component showed steeply dipping, dual-polarity directions, which passed a reversal test (positive, class 'C', McFadden & McElhinny 1990; Fig. 6).

IRM acquisition and hysteresis curves of representative samples were dominated by the response of the low-coercivity phase that saturated by 400 mT (Fig. 7). The bulk hysteresis properties (saturation coercivity $H_c \sim 10$ mT, ratios of coercivity of remanence to saturation coercivity $H_{cr}/H_c \sim 2$ and ratios of saturation remanence to saturation magnetization $M_{rs}/M_s \sim 0.15$) and a very slight 'wasp-waistedness' (Fig. 7b) can be interpreted as a mixture of a very small amount of a low-coercive coarse MD magnetite and high coercivity titanohaematite or ilmeno-haematite.

Similarly, two components are distinguished in the IRM acquisition curves (Fig. 7c): a lower coercivity phase (magnetite) that saturates by 100 mT and a harder component that starts to saturate above 100 mT and continues to acquire a small magnetization up to 4 T.

Low susceptibility values, high coercivity shown by AF demagnetization and high unblocking/Curie-Néel temperatures point to titanohaematite and minor haematite as the likely minerals carrying the remanent magnetization of Achala suite. Hysteresis and IRM properties indicate that rhombohedral oxides are accompanied by a low-coercivity phase (magnetite) in a very low proportion. The presence of even a small amount of magnetite in a high-field experiment masks the contributions from spin-canted haematite.

Thermal and AF demagnetization suggests that MD-magnetite is only a minor contributor to the NRM, carrying the soft fraction of remanence removed by 10–15 mT. The low magnetic saturation values mean that MD-magnetite is a very scarce mineral, though its rare presence dominates the high-field experiments because of its high saturation magnetization.

The temperature dependence of susceptibility ($k$–$T$) determined on whole rock samples is more sensitive to haematite as susceptibility is measured in low fields that do not produce magnetic saturation, and the resulting curve is not masked by magnetite. The $k$–$T$ curves show the presence of a mineral with Curie-Néel temperature of 620 °C, and a decay around $-30$ °C. This low temperature transition can be attributed to the Morin transition of pure haematite (Fig. 8). Haematite as magnetic carrier is in agreement with the very high bulk coercivity behaviour demonstrated by AF demagnetization.

In pure haematite, the change from paramagnetic to the antiferromagnetically order structure occurs at a Néel temperature of 680°C, but this temperature falls to about 480°C for a composition of $Ilm_{25}$ (Fig. 9). The measured Néel or Curie temperatures of 640–610 °C indicates the presence of $FeTiO_3$ in the haematite of Achala suite, of 6–10 per cent. The second unblocking temperature of 670–680 °C, observed in some samples, indicates the presence of some pure haematite, also indicated by the Morin transition observed in $k$–$T$ measurements.

The magnetic components carried by haematite and titanohaematite are used to calculate a paleomagnetic pole for the batholith. This pole fits the 380–360 Myr segment of the apparent polar wander path for the Paleozoic of Gondwana (Geuna *et al.* 2008b). Because it coincides with the crystallization age of 368 Myr obtained on zircons by Dorais *et al.* (1997), this pole position favours the interpretation that the titanohaematite formed during the primary crystallization and cooling and not as a product of a much later hydrothermal alteration.

## Mineral chemistry—petrography and chemistry of opaque oxides

Microscopic observation of polished sections permitted the identification of exsolved titanohaematite and haemo-ilmenite grains, in an abundance ranging from 0.5 to 1 volume per cent (Fig. 10). As expected, the rare magnetite indicated by the rock-magnetic procedures was not observed at the microscope scale.

Figs 10 and 11 illustrate the characteristic features seen in all three samples examined in polished sections in reflected light and in electron-backscatter images. They consist of two coexisting primary rhombohedral oxides—titanohaematite and ferri-ilmenite. During cooling, following magmatic crystallization, each of these oxides exsolved lamellae of the other to produce haemo-ilmenite (ilmenite with haematite exsolution) and ilmeno-haematite (haematite with ilmenite exsolution) in a fashion typical of many slowly cooled igneous and metamorphic rocks. Later, but still probably at relatively high temperature, there was an oxidation, likely related to varied local influx of cognate hydrothermal fluids. This process produced
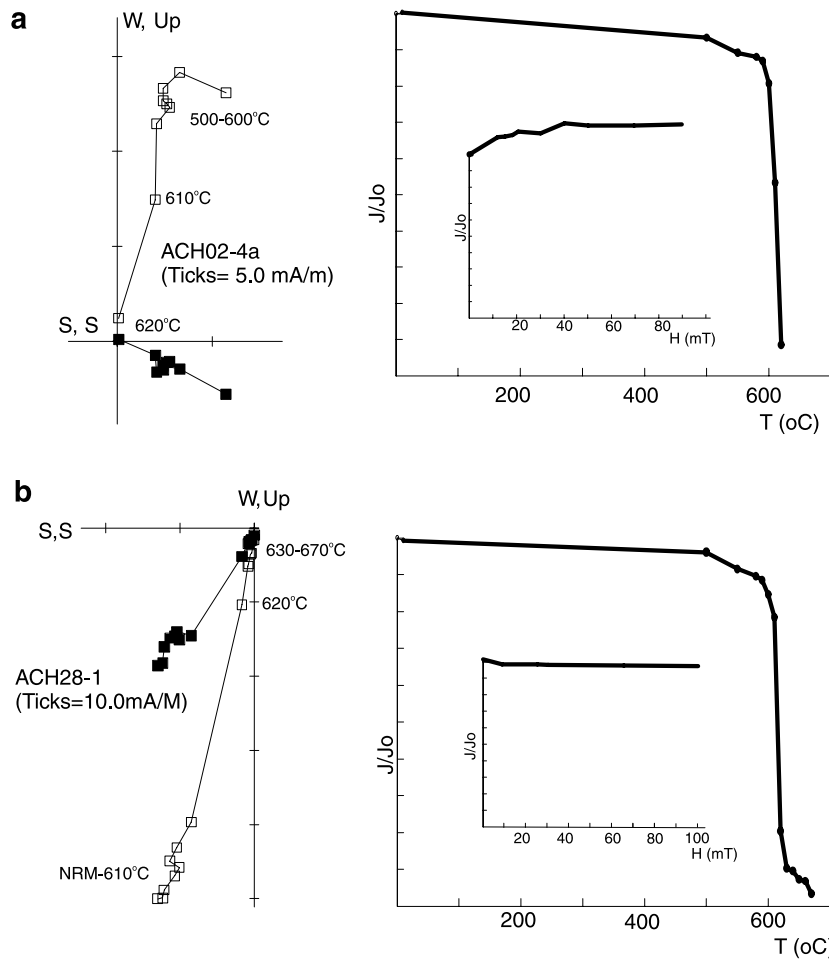
**Figure 4.** (left-hand panel) Vector endpoint diagrams and (right-hand panel) normalized intensity plots for thermal demagnetization from 0 to 680 °C, for two samples from Achala Batholith: (a) ACH2–4a, normal polarity and discrete unblocking temperature at 620 °C; (b) ACH28–1, reversed polarity and two discrete unblocking temperatures at 625 and 675 °C. On the demagnetization diagram open (solid) symbols indicate projection onto the vertical (horizontal) plane. Insets in normalized intensity plots show normalized alternating field demagnetization on the same specimens.
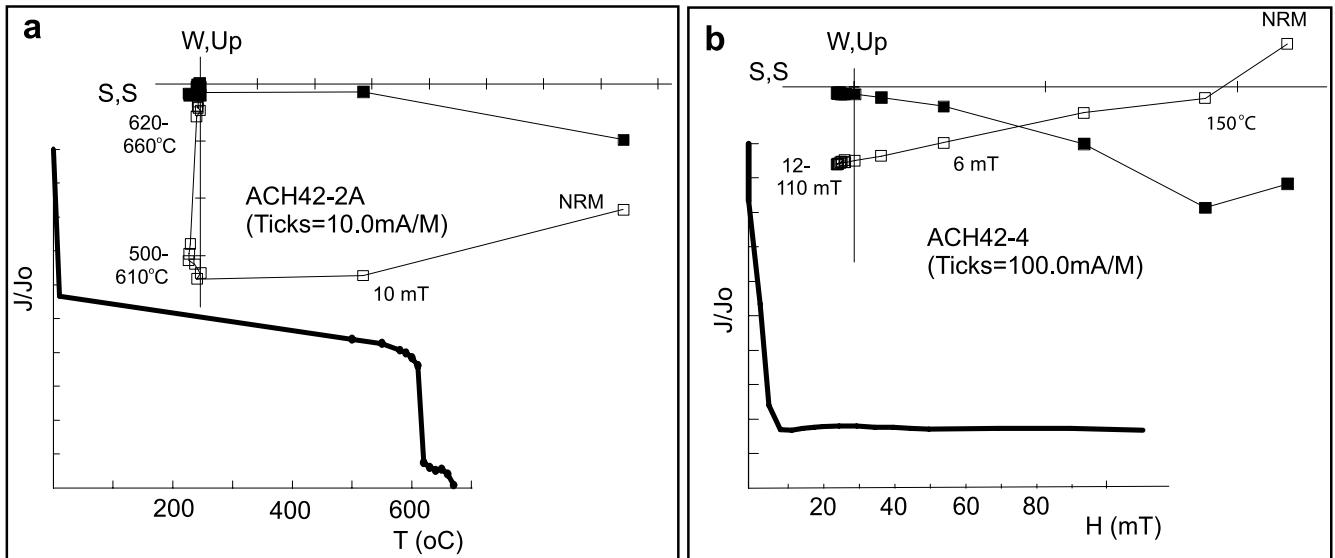


**Figure 5.** Vector endpoint diagrams and normalized intensity plots for thermal demagnetization from 0 to 680 °C for sample ACH42 from Achala Batholith. Symbols as in Fig. 4. AF demagnetization up to 15 mT removes a soft component that represents a fraction varying between 40 per cent (a) and 80 per cent (b) of the NRM, and is carried by trace amounts of MD magnetite. (a) Thermal demagnetization up to 680 °C, showing two discrete unblocking temperatures for a component carried by haematite; (b) AF demagnetization was ineffective to remove the high-temperature component.

© 2008 The Authors, *GJI*, **175,** 925–941
Journal compilation © 2008 RAS

**Table 1.** Rock magnetic results for Achala Batholith, 31°30′S, 64°45′W, Córdoba, Argentina.

| Site | N | MS | NRM | Tubl | per cent Rem 500 |
|------|---|------|--------|---------|------------------|
| 01 | 5 | 8.3 | 0.60 | 630/680 | 100 |
| 02 | 5 | 72.4 | 19.01 | 620 | 95 |
| 03 | 5 | 20.6 | 1.74 | 620 | 72 |
| 04 | 4 | 19.5 | 2.29 | 620/685 | 100 |
| 05 | 4 | 8.2 | 31.41 | 625 | 35 |
| 15 | 4 | 7.8 | 23.09 | 640 | 18 |
| 20 | 3 | 17.2 | 7.66 | 610/650 | 25 |
| 21 | 3 | 9.7 | 1.64 | 640/680 | 80 |
| 22 | 5 | 18.0 | 4.78 | 630/675 | 94 |
| 23 | 4 | 12.9 | 2.31 | 640/680 | 95 |
| 24 | 3 | 14.1 | 6.96 | 625/680 | 109 |
| 26 | 3 | 10.3 | 0.27 | 635/? | 63 |
| 27 | 5 | 17.1 | 1.34 | 625/670 | 90 |
| 28 | 4 | 38.2 | 45.45 | 625/675 | 100 |
| 29 | 4 | 53.3 | 5.21 | 625 | 27 |
| 38 | 5 | 44.9 | 21.43 | 625 | 120 |
| 40 | 5 | 11.6 | 1.97 | 620/680 | 70 |
| 42 | 5 | 50.6 | 220.50 | 615/670 | 40 |
| 46 | 3 | 9.9 | 0.58 | 615 | 33 |
| 50 | 4 | 73.5 | 31.30 | 625/670 | 100 |
| 113 | 6 | 7.1 | 4.58 | 640 | 100 |

*Notes:* N, Number of specimens; MS, Mean magnetic susceptibility $\times 10^{-5}$ (SI); NRM, Intensity of natural remanent magnetization, $\mathrm{mA\,m^{-1}}$; Tubl, Unblocking temperature as determined from thermal demagnetization of the NRM; per cent Rem500, Fraction of remanence remaining after thermal demagnetization up to 500 °C.
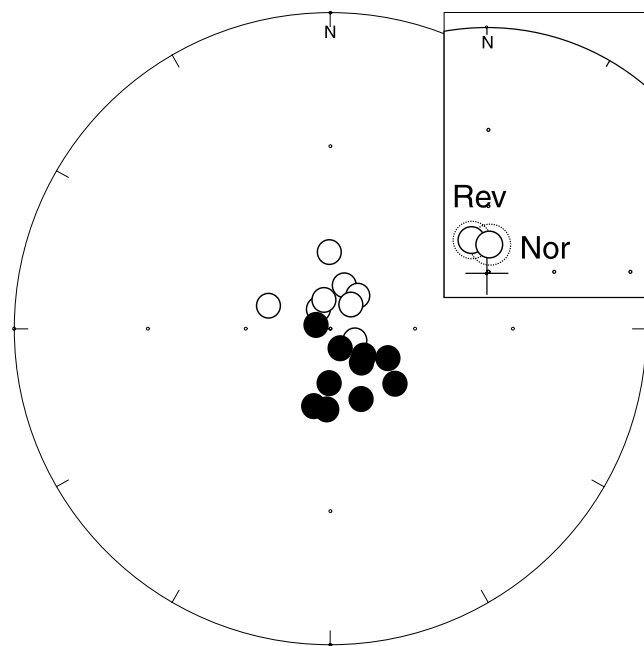


**Figure 6.** Paleomagnetic *in situ* site mean directions in stereographic projection. Open (solid) symbols indicate negative (positive) inclination. Inset depicts a positive (class C) reversal test for these paleomagnetic data (reversed directions inverted into normal directions, the outer circles represent the 95 per cent confidence cone).

complex local intergrowths of rutile + haematite + residual ilmenite replacing haemo-ilmenite (Figs 10e and f). At the same time, the oxidation reactions had a less obvious effect on ilmeno-haematite, usually showing minor invasion by needles of secondary rutile at the
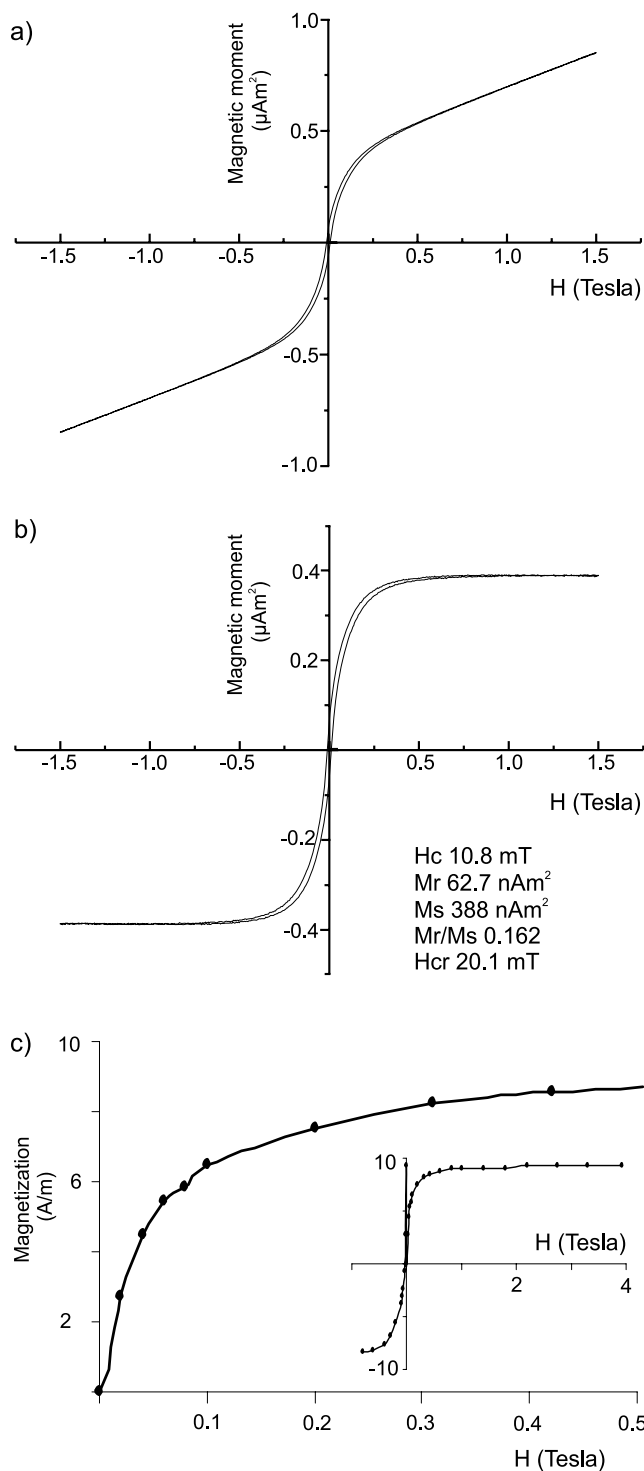


**Figure 7.** (a) Typical hysteresis curves, (b) is corrected for paramagnetic content. Note the slight constriction in the middle section of the curve (wasp-waistedness). (c) Acquisition of isothermal remanent magnetization (IRM) up to 0.5 T for a typical sample. Shown in inset is the IRM plot up to 4 T and backfield demagnetization of saturation IRM. The figure shows that response of strong-field experiments is mainly dominated by minor magnetite fraction.
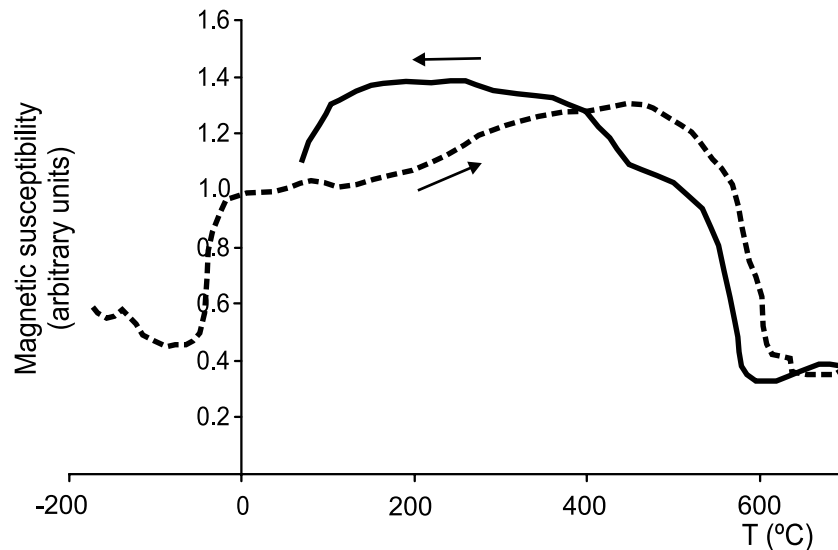
**Figure 8.** Typical low-field thermomagnetic ($k$–$T$) curves. Dashed line is for heating, and solid line is for cooling thermomagnetic curve.
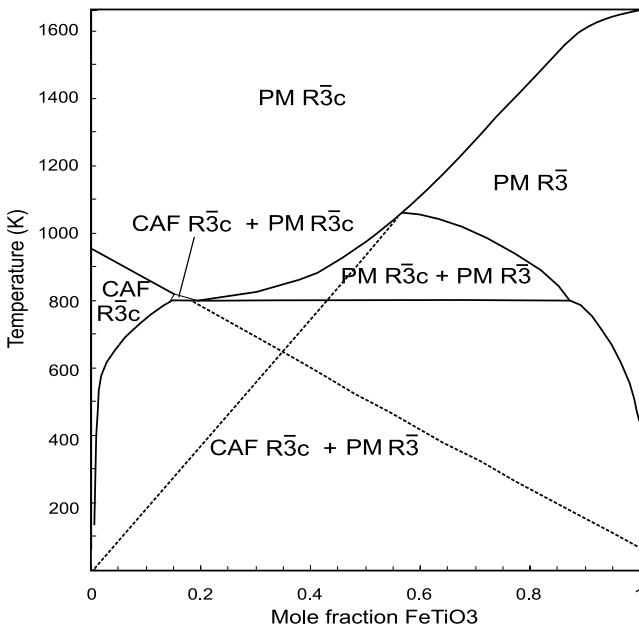


**Figure 9.** Summary of phase relations in the ilmenite–haematite solid solution at 1 atm, taken from McEnroe *et al.* (2007). R$\bar{3}c$, cation disordered; R$\bar{3}$, cation ordered; PM, paramagnetic; CAF, canted antiferromagnetic; FM, ferrimagnetic and AF, antiferromagnetic. The dashed lines show the metastable extension of the magnetic ordering transition and for the Fe–Ti chemical ordering transition for intermediate compositions, quenched from above the miscibility gap.

scale of the electron microprobe. This discrepancy is not surprising because a reaction with a fluid slightly more oxidizing than the ferri-ilmenite + titano-haematite assemblage would naturally be farther from equilibrium with the ferri-ilmenite than with the titano-haematite, hence more susceptible to reaction. However, combined evidence from the EMP analyses and magnetic experiments makes us suspect that the haematite may contain secondary rutile at the submicroscopic level.

In numerous grains the host and lamellae were coarse enough for effective EMP analyses (Tables 2 and 3). Host and lamellar

compositions are extremely similar to those in intergrowths of ilmenite and haematite studied previously (McEnroe & Brown 2000; McEnroe *et al.* 2001a,b, 2002, 2004, 2007; Kasama *et al.* 2004), with the exception that in these granite oxides, the dominant minor component in the ilmenite is pyrophanite (MnTiO$_3$). Representative weight percent analyses of the oxides are given in Table 2, for ilmenite host grains (haemo-ilmenite), and in Table 3, for the haematite host grains (ilmeno-haematite). Formulations are also expressed in terms of mole percent of end members or major component ratios. The key ratios are 'Ilm' = R$^{2+}$TiO$_3$/(R$^{2+}$TiO$_3$ + R$^{3+}_2$O$_3$) (where R$^{2+}$ = all divalent cations and R$^{3+}$ = all trivalent cations), also calculated more simply as 2Ti/(2Ti + R$^{3+}$) and pyrophanite = MnTiO$_3$/(R$^{2+}$TiO$_3$ + R$_2$O$_3$), alternatively expressed as Mn/[R$^{2+}$+(R$^{3+}$/2)] (see Robinson *et al.* 2001 for details on construction of these plots).

Unaltered ilmenite compositions are near end-member, ranging ilmenite$_{90-100}$, with most between ilm$_{96}$ and ilm$_{98}$ (Table 2). The pyrophanite component in all the good ilmenite analyses is very significant, ranging from 7 to 16 mole percent. Late enrichment in MnTiO$_3$ component is a likely effect in late stages of fractional crystallization of granitic magma, though the relatively high Fe$_2$O$_3$ component implies either unusual compositions in the sources or unusual environmental conditions. The titanohaematite host grains have compositions of ilm$_{25-15}$ (haematite$_{75-85}$) with minor amounts of V$_2$O$_3$, Al$_2$O$_3$ and Cr$_2$O$_3$. The most haematite rich analyses ilm$_{18-15}$ (hem$_{83-85}$) represent the least overlap.

The relationships between contents of Fe$_2$O$_3$, FeTiO$_3$ and MnTiO$_3$ are illustrated in Fig. 12. The vertical axis plots 2Ti/(2Ti + R$^{3+}$), which is the equivalent of the fraction of R$^{2+}$TiO$_3$ 'ilmenite' component to total R$^{2+}$TiO$_3$ + R$^{3+}_2$O$_3$. The horizontal axis Mn/[R$^{2+}$+(R$^{3+}$/2)] illustrates the fraction of MnTiO$_3$ (pyrophanite) substitution (see McEnroe *et al.* 2001b; Robinson *et al.* 2001, for discussion of plotting parameters in these diagrams). Like MgTiO$_3$ in rocks of more mafic composition, there is a very strong fractionation of MnO into the ilmenite and out of the substantial FeTiO$_3$ component of the haematite. However, the ilmenite contains a higher V$_2$O$_3$ component than does the coexisting haematite, in some ilmenites exceeding the amount of Fe$_2$O$_3$.

This is an uncommon feature because there is normally a strong fractionation of V$_2$O$_3$ into haematite. Probe analyses of the
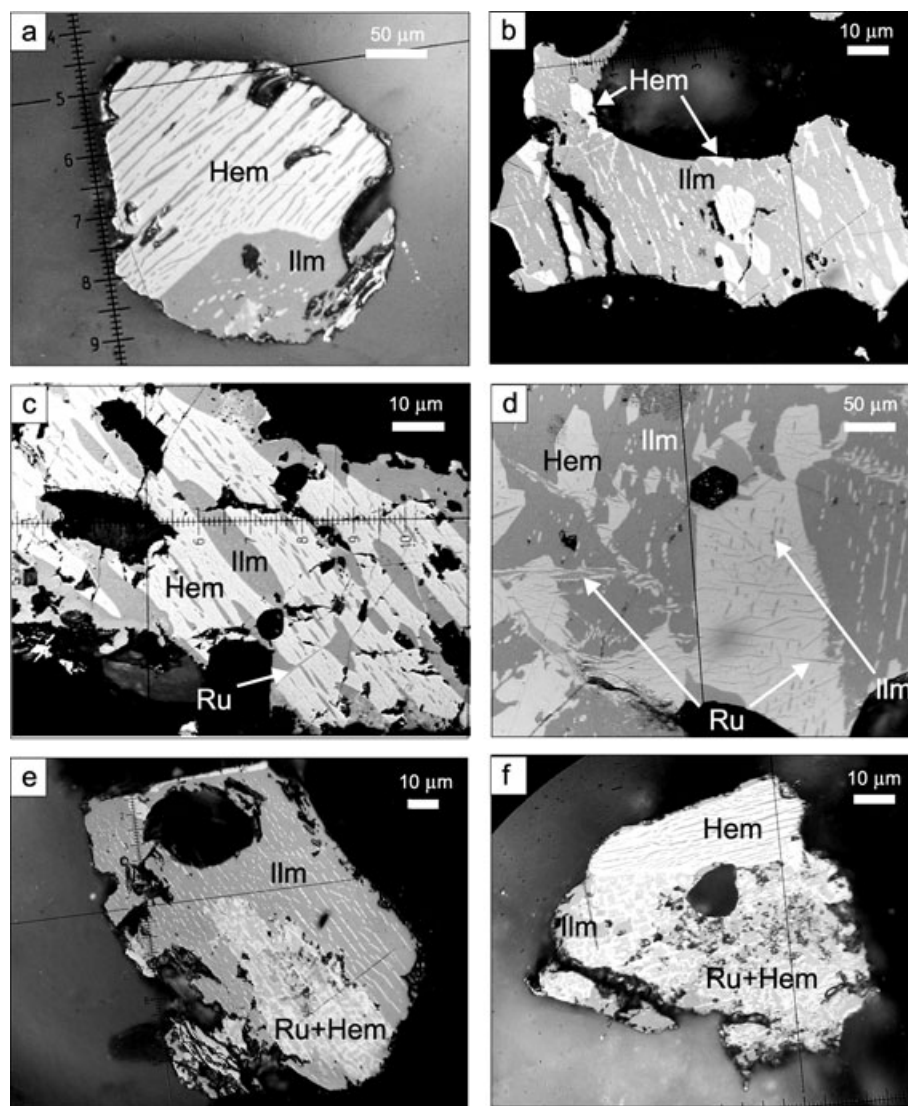
**Figure 10.** Photomicrographs of iron–titanium oxide occurrences in the Achala Batholith, in reflected light and under oil-immersion objectives. Although the oxide phases are heavily exsolved, they are labelled according to the host member, as follows: Ilm, ilmenite; Hem, haematite; Ru, rutile. (a) Oriented lamellae of ilmenite (dark grey) hosted by haematite (light grey). (b) Oriented lamellae of haematite (light grey) hosted by ilmenite (darker grey). (c) Larger ilmenite lamellae contain small lenses of haematite as a second generation exsolution. (d) Large titanohaematite area shows exsolution of rutile (medium grey) in blitz texture. (e) and (f) Dirty areas of low temperature haematite + rutile alteration.

secondary rutile-haematite-ilmenite intergrowths (Figs 10e and f) yield few 'acceptable' analyses, and most of these were for rutile. Likely the spatial relationships of the secondary phases are more complex than in the original higher-temperature exsolved intergrowths, so that most of the rhombohedral oxide analyses give poor totals, probably related to overlaps of very fine grains of rhombohedral oxides and rutile.

## DISCUSSION

Based on magnetic measurements, we concluded that ilmeno-haematite, haemo-ilmenite and haematite are the main magnetic minerals of the Achala Batholith, with ilmenite content in haematite restricted to 6–10 per cent. The ubiquitous presence of ilmeno-haematite and the virtual absence of magnetite are supported by thermal and alternating field demagnetization studies, saturation magnetization measurements, hysteresis properties and temperature-

hysteresis studies. Once the mechanism (and timing) of haematite formation is established, the petrological significance of this mineral will be able to be discussed.

## Mechanism and timing of titanohaematite formation

Half of the sites sampled in Achala suite's main facies showed a stable, double-polarity magnetic remanence carried by titanohaematite and haematite. These phases have been observed under the optical microscope as part of three assemblages: (1) the most abundant as a product of exsolution from members of the haematite-ilmenite solid solution series (Fig. 9); (2) as a part of secondary intergrowths of rutile-haematite-ilmenite produced by local oxidation of ilmenite host grains and (3) as part of the association haematite-rutile, a local low-temperature oxidation product of titanohaematite host grains.

Thermodynamic-experimental models predict the presence of a miscibility gap below 700–800 °C (Fig. 9), separating a
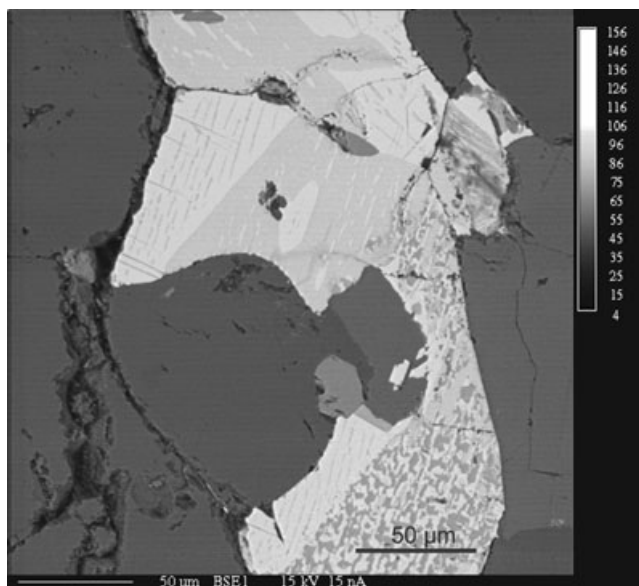
**Figure 11.** Electron backscatter image showing typical oxide grains in sample 2–3b and typical of all the samples. Brightest backscatter (lower right and top left hand panel) is shown by haematite with thin grey exsolution lamellae of darker ilmenite parallel to (001) and rare very thin cross cutting needles of rutile. Darker backscatter (upper centre) is shown by ilmenite with both thick and thin exsolution lamellae of haematite parallel to (001). Blotchy pattern (lower right hand panel) consists of rutile (darkest), haematite (lightest) and residual ilmenite (intermediate), which was produced by fluid mediated preferential oxidation of ilmenite. Surrounding darkest grey consists of silicates.

paramagnetic haematite-rich phase (PM $R\bar{3}c$) from a paramagnetic ilmenite-rich phase (PM $R\bar{3}$). At lower temperatures, the haematite-rich limb of the miscibility gap approaches the magnetic ordering transition, causing the PM $R\bar{3}c$ phase to become canted antiferromagnetic (CAF $R\bar{3}c$). Under equilibrium conditions, magnetic ordering in the haematite-rich phase leads to the eutectoid solid state reaction PM $R\bar{3}c \rightarrow$ CAF $R\bar{3}c$ + PM R$\bar{3}$, and a pronounced widening of the miscibility gap. Estimates of the temperature of the eutectoid reaction vary between ~390 °C (Ghiorso 1997; Harrison & Becker 2001; Robinson *et al.* 2004) and 520 °C (Burton 1985; Harrison 2006; McEnroe *et al.* 2007), whereas estimates of its position vary between 20 and 31 mole percent ilmenite (hem 80–69). The equilibrium state at lower temperatures consists of an intergrowth of CAF $R\bar{3}c$ and PM $R\bar{3}$ phases, with compositions that diverge toward pure haematite and pure ilmenite, respectively. The size distribution and spatial arrangement of these phases is a complex function of the cooling history.

The fact that the rocks found in the Achala Batholith contain two coexisting rhombohedral oxides implies crystallization below 700–800°C, followed by slow cooling with continued exsolution.

Unblocking temperatures of 610–640 °C indicate the presence of ~6–10 per cent ilmenite component in the $Fe_2O_3$ structure of the haematite, carrying the NRM. The experimentally determined Néel temperature of about 610–640 °C is related to the present compositions of the exsolved titanohaematite and haemo-ilmenite. The original titanohaematite prior to exsolution was much more Ti-rich and would have had a Néel temperature significantly lower than 610 °C.

Many of the haemo-ilmenite grains show extensive alteration, likely due to a fluid associated with cooling of the pluton. It is clear that exsolution of haematite and ilmenite occurred at relatively high

**Table 2.** Representative EMP analyses of ilmenite from samples 2–3b, 22–2b and 38–1b with structural formulae, calculated end members and plotting ratios.

| Wt per cent | 2–3b Ilmenite | | 22–2b Ilmenite | | 38–1b Ilmenite | |
|---|---|---|---|---|---|---|
| | 4–51 | 6–173 | 1–14 | 3a-34 | 3–29 | 3–35 |
| $SiO_2$ | 0.09 | 0.03 | 0.04 | 0.04 | 0.01 | 0.02 |
| $TiO_2$ | 50.81 | 50.61 | 51.35 | 51.41 | 51.62 | 51.23 |
| $Al_2O_3$ | 0.05 | 0.05 | 0.04 | 0.04 | 0.03 | 0.04 |
| $Cr_2O_3$ | 0 | 0 | 0 | 0 | 0.03 | 0.34 |
| $V_2O_3$ | 1.16 | 1.10 | 1.07 | 1.09 | 1.05 | 1.06 |
| $Fe_2O_3$[a] | 1.83 | 2.45 | 0.50 | 0.47 | 1.46 | 1.32 |
| MgO | 0.09 | 0.06 | 0.06 | 0.04 | 0.09 | 0.08 |
| NiO | 0 | 0 | 0 | 0 | 0 | 0 |
| FeO[a] | 41.56 | 41.19 | 38.94 | 40.93 | 42.12 | 41.61 |
| MnO | 3.90 | 4.16 | 7.07 | 5.19 | 4.10 | 4.28 |
| ZnO | 0.09 | 0 | 0.02 | 0.02 | 0 | 0.01 |
| CaO | 0.04 | 0.03 | 0 | 0 | 0 | 0 |
| Total | 99.61 | 99.68 | 99.09 | 99.22 | 100.50 | 99.68 |
| FeO[b] | 43.20 | 43.39 | 39.39 | 41.35 | 43.43 | 42.79 |
| Total[b] | 99.43 | 99.43 | 99.04 | 99.18 | 100.36 | 99.55 |
| Cations per 3 O atoms | | | | | | |
| Si | 0.0023 | 0.0008 | 0.0010 | 0.0010 | 0.0003 | 0.0005 |
| Ti | 0.9678 | 0.9640 | 0.9827 | 0.9828 | 0.9747 | 0.9752 |
| Al | 0.0015 | 0.0015 | 0.0012 | 0.0012 | 0.0009 | 0.0012 |
| Cr | | | | | 0.0006 | 0.0008 |
| V | 0.0236 | 0.0224 | 0.0218 | 0.0222 | 0.0211 | 0.0215 |
| $Fe^{3+}$ | 0.0348 | 0.0467 | 0.0096 | 0.0089 | 0.0276 | 0.0251 |
| Mg | 0.0034 | 0.0023 | 0.0023 | 0.0015 | 0.0034 | 0.0030 |
| $Fe^{2+}$ | 0.8802 | 0.8724 | 0.8287 | 0.8702 | 0.8844 | 0.8807 |
| Mn | 0.0837 | 0.0892 | 0.1524 | 0.1118 | 0.0872 | 0.0918 |
| Zn | 0.0017 | | 0.0004 | 0.0004 | | 0.0002 |
| Ca | 0.0011 | 0.0008 | | | | |
| Total | 2.0000 | 2.0000 | 2.0000 | 2.0000 | 2.0000 | 2.0000 |
| Calculated per centages of end members | | | | | | |
| $FeSiO_3$ | 0.228 | 0.076 | 0.102 | 0.102 | 0.025 | 0.051 |
| $MgTiO_3$ | 0.340 | 0.227 | 0.228 | 0.152 | 0.337 | 0.302 |
| $FeTiO_3$ | 87.794 | 87.165 | 82.763 | 86.920 | 88.412 | 88.024 |
| $MnTiO_3$ | 8.367 | 8.925 | 15.239 | 11.176 | 8.720 | 9.177 |
| $ZnTiO_3$ | 0.168 | | 0.038 | 0.038 | | 0.019 |
| $CaTiO_3$ | 0.109 | 0.081 | | | | |
| Sum | 97.005 | 96.473 | 98.369 | 98.386 | 97.494 | 97.571 |
| $Fe_2O_3$ | 1.741 | 2.334 | 0.482 | 0.445 | 1.379 | 1.255 |
| $Cr_2O_3$ | | | | | 0.030 | 0.040 |
| $V_2O_3$ | 1.179 | 1.119 | 1.089 | 1.108 | 1.053 | 1.074 |
| $Al_2O_3$ | 0.075 | 0.075 | 0.060 | 0.060 | 0.044 | 0.060 |
| Sum | 2.995 | 3.527 | 1.631 | 1.614 | 2.506 | 2.429 |
| Total | 100.000 | 100.000 | 100.000 | 100.000 | 100.000 | 100.000 |
| Plotting ratios | | | | | | |
| 2Ti/* | 0.9700 | 0.9647 | 0.9837 | 0.9838 | 0.9749 | 0.9757 |
| Cr/* | | | | | 0.0003 | 0.0004 |
| V/* | 0.0118 | 0.0112 | 0.0109 | 0.0111 | 0.0105 | 0.0107 |
| Al/* | 0.0007 | 0.0007 | 0.0006 | 0.0006 | 0.0004 | 0.0006 |
| Mn/# | 0.0837 | 0.0892 | 0.1524 | 0.1118 | 0.0872 | 0.0918 |

*Notes:*
[a] $Fe_2O_3$ and FeO back-calculated after determining stoichiometric formula.
[b] Total Fe as FeO as in original EMP analysis and original sum.
* $= 2Ti + R^{3+}$;. # $= R^{2+} + (R^{3+}/2)$.

temperatures of 675–520 °C and continued to at least 400 °C. It is also likely that an oxidizing fluid was associated with the later stages because the host haematite grains show less alteration than the host ilmenite grains. A result of these oxidizing conditions is late alteration of haemo-ilmenite to ilmenite + rutile + haematite and of titanohaematite producing rutile. These reactions would result

**Table 3.** Representative EMP analyses of haematite from samples 2–3b, 22–2b and 38–1b with structural formulae, calculated end members and plotting ratios.

| Wt per cent | 2–3b Haematite | | 22–2b Haematite | | 38–1b Haematite | |
|---|---|---|---|---|---|---|
| | 6–209 | 6–228 | 2a–1 | 2a–10 | 1a–18 | 2a–12 |
| $SiO_2$ | 0.06 | 0.05 | 0.03 | 0.07 | 0.07 | 0.06 |
| $TiO_2$ | 9.13 | 8.82 | 8.61 | 8.72 | 8.01 | 8.10 |
| $Al_2O_3$ | 0.07 | 0.06 | 0.03 | 0.02 | 0.06 | 0.03 |
| $Cr_2O_3$ | 0.05 | 0.08 | 0.04 | 0.03 | 0.05 | 0.04 |
| $V_2O_3$ | 0.54 | 0.56 | 0.56 | 0.60 | 0.43 | 0.50 |
| $Fe_2O_3$[a] | 81.05 | 81.76 | 83.78 | 82.68 | 84.48 | 84.53 |
| MgO | 0.01 | 0 | 0.02 | 0.01 | 0.01 | 0 |
| NiO | 0 | 0.04 | 0.02 | 0.01 | 0.01 | 0.03 |
| FeO[a] | 8.16 | 7.85 | 7.51 | 7.64 | 7.14 | 7.16 |
| MnO | 0.10 | 0.05 | 0.20 | 0.25 | 0.12 | 0.13 |
| ZnO | | 0.05 | | | | 0.04 |
| CaO | | 0.01 | 0.01 | | | |
| Total | 99.17 | 99.32 | 100.81 | 100.04 | 100.37 | 100.62 |
| FeO[b] | 81.09 | 81.41 | 82.89 | 82.04 | 83.15 | 83.22 |
| Total[b] | 91.05 | 91.13 | 92.41 | 91.75 | 91.91 | 92.15 |
| *Cations per 3 O atoms* | | | | | | |
| Si | 0.0016 | 0.0013 | 0.0008 | 0.0018 | 0.0018 | 0.0016 |
| Ti | 0.1821 | 0.1758 | 0.1691 | 0.1726 | 0.1581 | 0.1595 |
| Al | 0.0022 | 0.0019 | 0.0009 | 0.0006 | 0.0019 | 0.0009 |
| Cr | 0.0010 | 0.0017 | 0.0008 | 0.0006 | 0.0010 | 0.0008 |
| V | 0.0115 | 0.0120 | 0.0118 | 0.0127 | 0.0090 | 0.0104 |
| $Fe^{3+}$ | 1.6178 | 1.6303 | 1.6466 | 1.6372 | 1.6683 | 1.6657 |
| Mg | 0.0004 | | 0.0008 | 0.0004 | 0.0004 | |
| Ni | | 0.0009 | 0.0004 | 0.0002 | 0.0002 | 0.0006 |
| $Fe^{2+}$ | 0.1811 | 0.1739 | 0.1640 | 0.1682 | 0.1566 | 0.1568 |
| Mn | 0.0022 | 0.0011 | 0.0044 | 0.0056 | 0.0027 | 0.0029 |
| Zn | | 0.0010 | | | | 0.0008 |
| Ca | | 0.0003 | 0.0003 | | | |
| Total | 2.0000 | 2.0000 | 2.0000 | 2.0000 | 2.0000 | 2.0000 |
| *Calculated per centages of end members* | | | | | | |
| $FeSiO_3$ | 0.159 | 0.132 | 0.078 | 0.184 | 0.184 | 0.157 |
| $MgTiO_3$ | 0.040 | | 0.078 | 0.039 | 0.039 | |
| $Ni\,TiO_3$ | | 0.085 | 0.042 | 0.021 | 0.021 | 0.063 |
| $FeTiO_3$ | 17.948 | 17.253 | 16.322 | 16.638 | 15.481 | 15.522 |
| $MnTiO_3$ | 0.225 | 0.112 | 0.442 | 0.557 | 0.267 | 0.288 |
| $ZnTiO_3$ | | 0.098 | | | | 0.077 |
| $CaTiO_3$ | | 0.028 | 0.028 | | | |
| Sum | 18.372 | 17.709 | 16.990 | 17.440 | 15.992 | 16.108 |
| $Fe_2O_3$ | 80.890 | 81.515 | 82.331 | 81.861 | 83.414 | 83.283 |
| $Cr_2O_3$ | 0.052 | 0.084 | 0.041 | 0.031 | 0.052 | 0.041 |
| $V_2O_3$ | 0.576 | 0.598 | 0.591 | 0.637 | 0.450 | 0.522 |
| $Al_2O_3$ | 0.109 | 0.094 | 0.046 | 0.031 | 0.093 | 0.046 |
| Sum | 81.628 | 82.291 | 83.010 | 82.560 | 84.000 | 83.892 |
| Total | 100.000 | 100.000 | 100.000 | 100.000 | 100.000 | 100.000 |
| *Plotting ratios* | | | | | | |
| 2Ti/* | 0.1824 | 0.1760 | 0.1693 | 0.1729 | 0.1584 | 0.1598 |
| Cr/* | 0.0005 | 0.0008 | 0.0004 | 0.0003 | 0.0005 | 0.0004 |
| V/* | 0.0058 | 0.0060 | 0.0059 | 0.0064 | 0.0045 | 0.0052 |
| Al/* | 0.0011 | 0.0009 | 0.0005 | 0.0003 | 0.0009 | 0.0005 |
| Mn/# | 0.0022 | 0.0011 | 0.0044 | 0.0056 | 0.0027 | 0.0029 |

*Notes:*

[a]$Fe_2O_3$ and FeO back-calculated after determining stoichiometric formula.

[b]Total Fe as FeO as in original EMP analysis and original sum.

* $= 2Ti + R^{3+}$;. $\# = R^{2+} + (R^{3+}/2)$.

Thermal demagnetization and Néel temperatures indicate the dominant compositions are in the range of $ilm_{10–6}$ per cent ($ilm_{90–94}$); however, a minimum ilmenite component of 15 per cent was measured on the microprobe. This comparison implies that many EMP analyses are overlap analyses, between fine-scale lamellae and host grains, not resolvable at the scale of the EMP analytical beam. Such a discrepancy has been resolved by TEM-EDS on other fine oxide intergrowths (McEnroe *et al.* 2001a, 2002, 2004, 2007; Kasama *et al.* 2004) showing much lower ilmenite component for the haematite measured between fine lamellae.

The oxidation of the titanohaematite grains (ilmeno-haematite), shown by the production of rutile needles, probably had an additional effect at the submicroscopic level. This slightly more oxidizing reaction likely occurred during the cooling of the intrusion and locally converted ilmenite component to rutile, affecting the interfaces between the ilmenite lamellae and titanohaematite host. This process would result in a decrease in NRM intensity because the magnetic moments at interfaces of the ilmenite and titanohaematite would be destroyed when ilmenite is converted to rutile. A simple balanced equation (here in oxygen proportions ∼volume) of Ilm16 + Oxygen, producing a more ilmenite-poor haematite plus rutile is

$$98.96\ Ilm16 + 1.04\ O = 95.83\ Ilm10 + 4.17\ TiO_2.$$
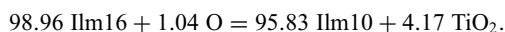
In addition to the above process, the oxidation to the haemo-ilmenite grains would also result in a decrease in remanent magnetization. In all cases, the NRM is a chemical remanent magnetization (CRM) acquired during cooling of the granite either by primary exsolution, or later, by alteration of the lamellae and hosts by the late-stage oxidizing fluids.

The coincidence of the paleomagnetic pole of the Achala batholith with the 380–360 Myr segment of the Apparent Polar Wander Path for the Paleozoic of Gondwana (Geuna *et al.* 2008b) favours the interpretation that the ilmeno-haematite and haemo-ilmenite formed early during the crystallization process and during cooling were subjected to a deuteric alteration under slightly more oxidizing conditions than the original magma.

## Petrology of Achala batholith

Previously the Achala Batholith has been ascribed to an S-type origin (i.e. magma derived from melting of metasedimentary rocks), based on peraluminosity and other mineralogical and chemical criteria (Lira & Kirschbaum 1990; Martino & Kirschbaum 1993; Lira *et al.* 1996; Dorais *et al.* 1997). Patiño Douce (1999) has established experimentally that only peraluminous leucogranites can be the result of pure crustal melts. Any other group of peraluminous granites requires the influx of substantial basaltic material. Therefore, even for traditionally considered S-type granites, a mantle contribution has to be expected. As for the Achala batholith, the mantle contribution is reflected in the presence of tonalite nodules (Lira & Kirschbaum 1990) and also in the $^{87}Sr/^{86}Sr$ ratios, which are locally too low (Rapela *et al.* 1990).

However, Achala batholith has a higher oxidation ratio compared with the classic S-type granites of the Lachlan Fold Belt (Fig. 2). The Achala oxidation ratio is not only higher than the expected for ilmenite-series granitoids, but also is higher than I-type, magnetite-series granitoids of the neighbouring and nearly coeval Renca batholith (Fig. 2).

Although the dominant Fe-Ti oxide is ilmenite, it does not occur pure as is typical in ilmenite-series granitoids but as an oxidized ilmenite-haematite solid solution. Haematite exsolution lamellae in
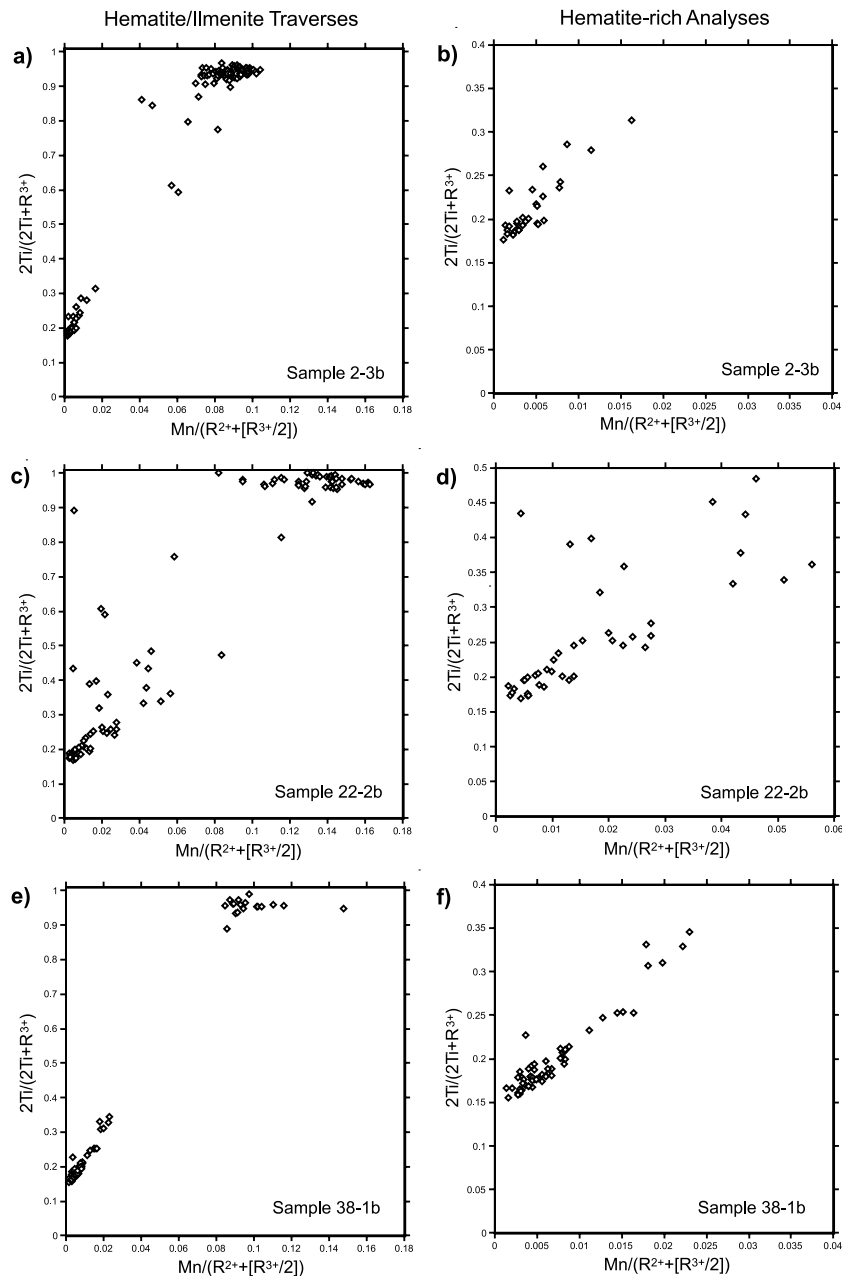
in a significant reduction of NRM intensities. Similar compositions of exsolved titanohaematites, with high coercivities have been reported (McEnroe & Brown 2000; McEnroe *et al.* 2001a); however, the NRM values from the Achala samples are markedly lower.

**Figure 12.** Plot of accepted analyses from traverses across haematite-ilmenite. Panels in the right-hand side show close-ups of figures in the left-hand panel, showing only haematite-rich compositions. (a) Sample 2–3b shows a concentration of Ilmenite compositions with 'Ilm' = 90–97 and haematite compositions with 'Ilm' = 17–20. Also shows the range of $MnTiO_3$ contents of ilmenite 7–10.5 and, particularly, shows the very low $MnTiO_3$ substitution in the $FeTiO_3$ content of haematite. Scattered analyses in centre of diagram are due to mineral overlaps. (b) This shows the few analyses with no overlap on adjacent ilmenite lamellae in sample 2–3b ranging from Ilm20–17.5 (hem 82.5–80). (c) Sample 22–2b, traverses across titano haematite, with coarse ilmenite lamellae showing a concentration of Ilmenite compositions with 'Ilm' = 95–100 and titanohaematite compositions with Ilm21–17 (hem83–79). Here the $MnTiO_3$ is much larger than in the other samples, but haematites show a very restricted range. The $MnTiO_3$ variations in accepted analyses seem to be partly primary variations in original ilmenite hosts with $MnTiO_3$ 12–16. However, within rutile-rich patches there are no 'accepted' ilmenite analyses. Scattered analyses in centre of diagram are due to mineral overlaps. (d) Close-up of part of c), the range of $MnTiO_3$ is related to ilmenite overlaps, and analyses with most ilmenite-poor compositions Ilm 20–17 and show very low $MnTiO_3$. (e) Sample 38–1b shows a concentration of Ilmenite compositions, with 'Ilm' = 94–98, and haematite compositions, with Ilm 21–15 (hem85–79). Areas analysed contained more haematite than ilmenite, reflected in the density of analyses. $MnTiO_3$ content of ilmenite is similar to sample 2–3b, typically 8.5–11.8. Scattered analyses in centre of diagram are due to mineral overlaps. (f) The very abundant haematite analyses converge on a very low $MnTiO_3$ content for the most haematite-rich compositions, where Ilm content is 20 to as low as 15.

ilmenite have been described only in oxidized I-type granites, usually accompanying magnetite (Whalen & Chappel 1988); however, magnetite is virtually absent in Achala samples.

The oxidized character of ilmenite correlates with the character of the whole-rock, as evidenced in the high oxidation ratio (Fig. 2).

Because felsic magmatic provinces in which intrusions are characterized by oxidation states that broadly span the boundary between magnetite- and ilmenite-series are gold prospective (Thompson *et al.* 1999; Blevin 2005), it is important to establish the origin and implications of the Achala oxidation state. In the studied
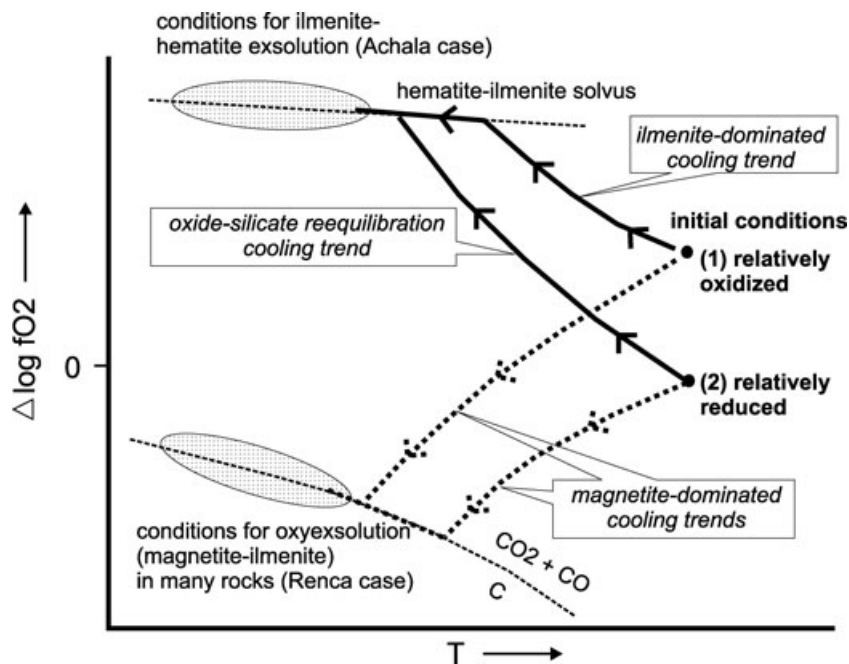
**Figure 13.** $\Delta\log f O_2$–T diagram showing inferred cooling trends for Fe–Ti oxides, after Frost (1991). Conditions for ilmenite-haematite exsolution can be reached from either relatively oxidized or relatively reduced initial conditions [dots labelled (1) and (2), respectively]. Oxidizing cooling path from condition (1) requires ilmenite-dominated cooling (magnetite absent); oxidation from (2) requires silicate-oxide reequilibration in presence of an $H_2O$-rich fluid.

examples from the Achala batholith, it appears that titanohaematite was crystallizing directly from the magma.

The T–$f O_2$ path, followed during cooling of an oxide assemblage, depends upon many factors, including original oxygen fugacity of the assemblage, the relative abundance of titanomagnetite and ilmenite and composition of the fluid (Frost 1991). A rock that crystallized at relatively oxidized conditions, but containing ilmenite as the major oxide, will follow a relatively oxidizing cooling trend (Frost 1991; Path 1 in Fig. 13). On cooling the $f O_2$ may reach that of the ilmenite-haematite solvus, causing haematite to exsolve from the ilmenite. In this scenario, the departure of the classic magnetite-ilmenite oxide assemblage would be due to the original absence of magnetite because of the stabilization of ilmenite at high $f O_2$ instead of magnetite, due to high Mn contents (Czamanske et al. 1977). High Mn contents in ilmenite have also been reported for Inti Huasi granite, south of Achala (Otamendi et al. 2002), and for the crystalline basement intruded by these Devonian granitoids (Zaccarini et al. 2004).

The Achala batholith departs from this trend in that both titanohaematite and a ferrian ilmenite were crystallizing together, from a melt that was already oxidized, and with cooling, the titanohaematite exsolved ilmenite lamellae and the ferrian ilmenite exsolved haematite lamellae.

For granites, another possible cooling path is one that is controlled by oxide-silicate reaction, rather than being controlled by interoxide equilibration (Frost 1991; Path 2 in Fig. 13). In granitoids with an $H_2O$-rich fluid, the major re-equilibration is likely to be reaction between the oxides, K-feldspar and biotite. This reaction has a relatively oxidizing trend with cooling and can cause rocks of a wide range of primary conditions to be oxidized to the haematite-ilmenite solvus.

The primary assemblage, with both titanohaematite and ferrian ilmenite, demonstrate the oxidizing nature of the original magma. Locally, a later and slightly more oxidizing fluid produced rutile

and haematite from the haemo-ilmenite and rutile from the titanohaematite. This process had important consequences for the rock magnetism of the Achala batholith. The final oxide assemblage is more oxidized than for a magnetite-ilmenite assemblage.

It is not uncommon to find haematite as part of the opaque mineral assemblage of granites. However, it is usually found accompanying magnetite as part of an oxidized assemblage (e.g. Ashwal & Hargraves 1977; Ellwood et al. 1980; Czamanske et al. 1981; Hagstrum & Johnson 1986; Dillet & Czamanske 1987; Whalen & Chappell 1988). The magnetite found in granites is usually coarse-grained and is capable of carrying a magnetic remanence of relatively high intensity, though relatively unstable. The peculiarity in Achala is to find the exsolved haematite-ilmenite alone. The absence of large discrete grains of magnetite makes these rocks very interesting from the paleomagnetic point of view because haematite is capable of carrying a very stable CRM acquired during early stages of cooling (Geuna et al. 2008b), and this is free of the undesirable masking effects of re-equilibrated, coarse-grained, pure magnetite.

Heavily exsolved ilmeno-haematite and haemo-ilmenite have been reported, associated with high remanence intensity, which was attributed to a particular mode of magnetization—lamellar magnetism (McEnroe et al. 2001a,b, 2002; Robinson et al. 2002, 2004). However, the magnetization of Achala batholith is unexpectedly low compared with those other samples showing lamellar magnetism. The secondary rutile-haematite-ilmenite intergrowths in the titanohaematite, and the alteration to the haemo-ilmenite grains may explain the reduced magnetization. In addition, there may be less of the very fine exsolution lamellae in the Achala rocks as compared to the previous studies cite above, possibly caused by a different cooling history or by lamellar coarsening during the hydrothermal event. Another possibility is that there is more alteration at a finer scale, in the ilmeno-haematite, than observed at the scale of the microprobe.

The ancient magnetic remanence, carried by primary ilmeno-haematite and haemo-ilmenite, is a good indication that magma was oxidized. The Achala cooling path has to have been different from that followed by Renca batholith, as Renca crystallized in $f O_2$–T conditions, entirely within the magnetite stability field.

## CONCLUSIONS

(1) Based on susceptibility values, Achala rocks can be classified as paramagnetic and part of the ilmenite-series following Ishihara (1981). The very low values of MS (MS $< 1 \times 10^{-3}$ SI) indicate that magnetite, if present, is very rare ($<0.02$ volumeper cent).

(2) The mineral carrying magnetic remanence is titanohaematite in ilmeno-haematite or haemo-ilmenite intergrowths, with discrete unblocking temperatures of $610$–$640\,°C$. The ilmenite component in haematite based on magnetic measurements is 6–10 per cent; EMP data gives compositions of 15–20 per cent ilmenite, suggesting that EMP data reflects areas in the titanohaematite host grains with submicroscopic Ti-rich lamellae.

(3) Achala samples contain titanohaematite, and ferri- ilmenite both as primary igneous phases, implying crystallization below $675°C$, with exsolution continuing to low temperatures ($<400°C$). The main exsolution features were produced during cooling from high-temperature magmatic conditions. Oxidizing conditions continued into the subsolidus, causing late-stage reactions of ilmenite host grains to ilmenite + rutile+ haematite and titanohaematite to ilmenite-poorer haematite + rutile. These reactions resulted in low susceptibility values and a strong reduction of NRM intensities.

(4) Pyrophanite component in ilmenite is very significant, ranging from 7 to 16 mole percent. Late enrichment in $MnTiO_3$ component is a likely effect in late stages of fractional crystallization of granitic magma, though the relatively high $Fe_2O_3$ component implies either unusual compositions in the sources, or unusual environmental conditions.

(5) The classic ilmenite-series granitoids are relatively reduced and weakly magnetic, and $f O_2$ is too low to crystallize magnetite. However, the weak MS of the Achala batholith is not due to reducing conditions but to strong oxidation, which prevented magnetite crystallization.

(6) The magnetic remanence was acquired during cooling, relatively soon after crystallization because the paleomagnetic pole obtained from the Achala batholith is coincident with Devonian Gondwana poles and in agreement with the zircon age of 368 Myr.

## ACKNOWLEDGMENTS

## REFERENCES

Ashwal, L.D. & Hargraves, R.B., 1977. Paleomagnetic evidence for tectonic rotation of the Belchertown pluton, West Central Massachussets, *J. geophys. Res.* **82**(8), 1315–1324.

Blevin, P.L., 1994. Magnetic susceptibility of the Lachlan Fold Belt and New England Batholith granites, AMIRA project P147B, final report (unpublished).

Blevin, P.L., 2003. Metallogeny of granitic rocks, in *Magmas to Mineralisation: the Ishihara Symposium*, pp. 1–4, eds Blevin, P., Jones, M. & Chappell, B., Geoscience Australia, Record 2003/14.

Blevin, P.L., 2005. Intrusion related gold deposits, Geoscience Australia open files, available at www.ga.gov.au/about/corporate/ga_authors/Expl_models/PL_Blevin_IRGD.jsp

Blevin, P.L. & Chappell, B.W., 1995. Chemistry, origin, and evolution of mineralized granites in the Lachlan Fold Belt, Australia: the metallogeny of I- and S-type granites, *Econ. Geol.,* **90,** 1604–1619.

Burton, B.P., 1985. Theoretical analysis of chemical and magnetic ordering in the system $Fe_2O_3$-$FeTiO_3$, *Am. Mineral.,* **72,** 329–336.

Chappell, B.W. & White, A.J., 1974. Two contrasting granite types, *Pacific Geol.,* **8,** 173–174.

Clark, D.A., 1997. Magnetic petrophysics and magnetic petrology: aids to geological interpretation of magnetic surveys, *AGSO J. Aust. Geol. Geophys.,* **17,** 83–103.

Clark, D.A., 1999. Magnetic petrology of igneous intrusions: implications for exploration and magnetic interpretation, *Expl. Geophys.,* **30,** 5–26.

Czamanske, G.K., Wones, D.R. & Eichelberger, J.C., 1977. Mineralogy and petrology of the intrusive complex of the Pliny Range, New Hampshire, *Am. J. Sci.,* **277,** 1073–1123.

Czamanske, G.K., Ishihara, S. & Atkin, S.A., 1981. Chemistry of rock-forming minerals of the Cretaceous-Paleocene Batholith in Southwestern Japan and implications for magma genesis, *J. geophys. Res.,* **86**(B11), 10 431–10 469.

de Patiño, M.G., 1989. Estudio geológico y petrológico del Batolito de Pampa de Achala, provincia de Córdoba, a los $31° 35'$ de latitud sur, *Unpublished thesis*. Facultad de Ciencias Exactas y Naturales, Universidad de Buenos Aires, 235 pp.

de Patiño, M.G. & Patiño Douce, A.E., 1987. Petrología y petrogénesis del Batolito de Achala, provincia de Córdoba, a la luz de la evidencia de campo, *Revista de la Asociación Geológica Argentina* **42**(1–2), 201–205.

Demange, M., Álvarez, J.O., López, L. & Zarco, J.J., 1996. The Achala Batholith (Córdoba, Argentina): a composite intrusion made of five independent magmatic suites. Magmatic evolution and deuteric alteration, *J. South Am. Earth Sci.,* **9**(1–2), 11–25.

Dillet, B. & Czamanske, G.K., 1987. Aspects of the petrology, mineralogy and geochemistry of the granitic rocks associated with Questa Caldera, northern New Mexico, USGS Open-file Report 87–258, 238 p.

Dorais, M.J., Lira, R., Chen, Y. & Tingey, D., 1997. Origin of biotite-apatite-rich enclaves, Achala batholith, Argentina, *Contrib. Mineral. Petrol.,* **130,** 31–46.

Ellwood, B.B., Whitney, J.A., Wenner, D.B., Mose, D. & Amerigian, C., 1980. Age, paleomagnetism, and tectonic significance of the Elberton Granite, Northeast Georgia Piedmont, *J. geophys. Res.,* **85**(B11), 6521–6533.

Frost, B.R., 1991. Magnetic petrology: factors that control the occurrence of magnetite in crustal rocks, in *Oxide Minerals: Petrologic and Magnetic Significance,* Reviews in Mineralogy, Vol. 25, pp. 489–509, Lindsley, D.H., Reviews in Mineralogy, **25,** 489–509.

Frost, B.R. & Lindsley, D.H., 1991. Occurrence of iron-titanium oxides in igneous rocks, in *Oxide Minerals: Petrologic and Magnetic Significance,* Reviews in Mineralogy, Vol. 25, pp. 433–468, ed Lindsley, D.H., Reviews in Mineralogy, **25,** 433–468.

Geoscience Australia, 2007. OZCHEM National Whole Rock Geochemistry data, available at http://www.ga.gov.au/gda/index.jsp

Geuna, S.E., Escosteguy, L.D., Miró, R., Candiani, J.C. & Gaido, M.F., 2008a. La susceptibilidad magnética del batolito de Achala (Devónico, Sierra Grande de Córdoba), y sus diferencias con otros granitos

"Achalianos", *Revista de la Asociación Geológica Argentina,* **63**(3), 380–394.

Geuna, S.E., Escosteguy, L.D. & Miró, R., 2008b. Palaeomagnetism of the Late Devonian – Early Carboniferous Achala Batholith, Córdoba, central Argentina: implications for the apparent polar wander path of Gondwana, *Gondwana Res.,* **13**(2), 227–237.

Ghiorso, M.S., 1997. Thermodynamic analysis of the effect of magnetic ordering on miscibility gaps in the FeTi cubic and rhombohedral oxide minerals and the FeTi oxide geothermometer, *Phys. Chem. Minerals,* **25**, 28–38.

Hagstrum, J.T. & Johnson, C.M., 1986. A paleomagnetic and stable isotope study of the pluton at Rio Hondo near Questa, New Mexico: implications for CRM related to hydrothermal alteration, *Earth planet. Sci. Lett.,* **78**, 296–314.

Harrison, R.J., 2006. Microstructure and magnetism in the ilmenite-hematite solid solution: A Monte Carlo simulation study, *The Am. Mineral.,* **91**(7), 1006–1024.

Harrison, R.I. & Becker, U., 2001. Magnetic ordering in solid solutions, *Euro. Mineral. Un. Notes Mineral.,* **3**, 349–383.

Introcaso, A., Lion, A. & Ramos, V.A., 1987. La estructura profunda de las sierras de Córdoba, *Revista de la Asociación Geológica Argentina,* **42**(1–2), 177–187.

Ishihara, S., 1981. The granitoid series and mineralization, *Econ. Geol.* **75th Anniversary Volume,** 458–484.

Jordan, T.E., Zeitler, P., Ramos, V. & Gleadow, A.J.W., 1989. Thermochronometric data on the development of the basement peneplain in the Sierras Pampeanas, Argentina, *J. South Am. Earth Sci.,* **2**(3), 207–222.

Kasama, T., McEnroe, S.A., Ozaki, N., Kogure, T. & Putnis, A., 2004. Effects of nanoscale exsolution in hematite-ilmenite on the acquisition of stable natural remanent magnetization, *Earth Planet. Sci. Lett.,* **224**, 461–475.

Lira, R. & Kirschbaum, A.M., 1990. Geochemical evolution of granites from the Achala batholith of the Sierras Pampeanas, Argentina, in *Plutonism from Antarctica to Alaska,* Vol. 241, pp. 67–76, eds Kay, S.M. & Rapela, C.W.. Geological Society of America Special Paper.

Lira, R., Ripley, E.M. & Españón, A.I., 1996. Meteoric water induced selvage-style greisen alteration in the Achala Batholith, central Argentina, *Chem. Geol.,* **133**, 261–277.

López de Luchi, M.G., 1986. Geología y petrología del basamento de la sierra de San Luis, región del Batolito de Renca, *Unpublished thesis.* Facultad de Ciencias Exactas y Naturales, Universidad de Buenos Aires, 374 pp.

López de Luchi, M.G., 1996. Enclaves en un batolito postectónico: petrología de los enclaves microgranulares del batolito de Renca, *Revista de la Asociación Geológica Argentina,* **51**(2), 131–146.

López de Luchi, M.G., Rapalini, A.E., Rossello, E. & Geuna, S., 2002. Rock and magnetic fabric of the Renca Batholith (Sierra de San Luis, Argentina): constraints on emplacement, *Lithos,* **61**, 161–186.

López de Luchi, M.G., Rapalini, A.E., Siegesmund, S. & Steenken, A., 2004. Application of magnetic fabrics to the emplacement and tectonic history of Devonian granitoids in central Argentina, in *Magnetic Fabric: Methods and Applications,* Vol. 238, pp. 447–474, eds Martín-Hernández, F., Lüneburg, F., Aubourg, C. & Jackson, M., Geological Society, London, Special Publications.

Martino, R.D. & Kirschbaum, A.M., 1993. Petrografía y composición química de una aplita granatífera en el borde occidental del Batolito de Achala. 12° Congreso Geológico Argentino y 2° Congreso de Exploración de Hidrocarburos, *Actas* **4**, 30–32.

McEnroe, S.A. & Brown, L.L., 2000. A closer look at remanence-dominated anomalies: rock-magnetic properties and magnetic mineralogy of the Russell Belt microcline-sillmanite gneisses, Northwest Adirondacks Mountains, New York, *J. geophys. Res.,* **105**, 16 437–16 456.

McEnroe, S. A., Harrison, R.J., Robinson, P., Golla, U. & Jercinovic, M.J., 2001a. The effect of fine-scale microstructures in titanohematite on the acquisition and stability of NRM in granulite facies metamorphic rocks from southwest Sweden, *J. geophys. Res.,* **106**, 30 523–30 546.

McEnroe, S.A., Robinson, P. & Panish, P.T., 2001b. Aeromagnetic anomalies, magnetic petrology, and rock magnetism of hemo-ilmenite- and

magnetite-rich cumulate rocks from the Sokndal Region, South Rogaland, Norway, *Am. Mineral.,* **86**, 1447–1468.

McEnroe, S.A., Harrison, R.J., Robinson, P. & Langhorst, F., 2002. Nanoscale haematite-ilmenite lamellae in massive ilmenite rock: an example of lamellar magnetism with implications for planetary magnetic anomalies, *Geophys. J. Int.,* **151**(3), 890–912.

McEnroe, S.A., Langenhorst, F., Robinson, P., Bromiley, G.D. & Shaw, C.S.J., 2004. What's magnetic in the lower Crust? *Earth planet. Sci. Lett.,* **226**, 175–192.

McEnroe, S.A., Robinson, P., Langenhorst, F., Frandsen, C., Terry, M.P. & Boffa Ballaran, T., 2007. Magnetization of exsolution intergrowths of hematite and ilmenite: Mineral chemistry, phase relations, and magnetic properties of hemo-ilmenite ores with micron- to nanometer-scale lamellae from Allard Lake, Quebec, *j. geophys. Res.,* **112**(B10103), doi:10.1029/2007JB004973.

McFadden, P.L. & McElhinny, M.W., 1990. Classification of the reversal test in palaeomagnetism, *Geophys. J. Int.,* **103**, 725–729.

Otamendi, J.E., Fagiano, M.R., Nullo, F.E. & Castellarini, P.A., 2002. Geología, petrología y mineralogía del granito Inti Huasi, sur de la sierra de Comechingones, Córdoba, *Revista de la Asociación Geológica Argentina,* **57**(4), 389–403.

Patiño Douce, A.E., 1999. What do experiments tell us about the relative contributions of crust and mantle to the origin of granitic magmas? in *Understanding Granites: Integrating New and Classical Techniques,* Vol. 168, pp. 55–75, eds Castro, A., Fernández, C. & Vigneresse, J.L., Geological Society of London, Special Publication.

Pinotti, L.P., Coniglio, J.E., Esparza, A.M., D'Eramo, F.J. & Llambías, E.J., 2002. Nearly circular plutons emplaced by stoping at shallow crustal levels, Cerro Aspero batholith, Sierras Pampeanas de Córdoba, Argentina, *J. South Am. Earth Sci.,* **15**, 251–265.

Pinotti, L., Tubía, J.M., D'Eramo, F., Vegas, N., Sato, A.M., Coniglio, J. & Aranguren, A., 2006. Structural interplay between plutons during the construction of a batholith (Cerro Aspero batholith, Sierras de Córdoba, Argentina), *J. Struct. Geol.,* **28**, 834–849.

Rapela, C.W., Heaman, L.M. & McNutt, R.H., 1982. Rb-Sr geochronology of granitoid rocks from the Pampean Ranges, Argentina, *J. Geol.,* **90**, 574–582.

Rapela, C.W., Toselli, A., Heaman, L. & Saavedra, J., 1990. Granite plutonism of the Sierras Pampeanas; an inner cordilleran Paleozoic arc in the Southern Andes, in *Plutonism from Antarctica to Alaska,* Vol. 241, pp. 77–90, eds Kay, S.M.. & Rapela, C.W.. Geological Society of America Special Paper 241.

Rapela, C.W., Pankhurst, R.J., Kirschbaum, A. & Baldo, E.G.A., 1991. Facies intrusivas de edad carbónica en el Batolito de Achala: evidencia de una anatexis regional en las Sierras Pampeanas? 6° Congreso Geológico Chileno, Actas, 40–45.

Rapela, C.W., Pankhurst, R.J., Casquet, C., Baldo, E., Saavedra, J. & Galindo, C., 1998. The Pampean Orogeny of the southern Proto-Andes: Cambrian continental collision in the Sierras de Córdoba, in *Proto-Andean margin of Gondwana,* eds Pankhurst, R.J. and Rapela, C.W., pp. 181–217. Geological Society of America Special Publication 142.

Robinson, P., Panish, P. & McEnroe, S.A., 2001. Minor element chemistry of hemo-ilmenite and magnetite-rich cumulates from the Sokndal Region, South Rogaland, Norway, *Am. Mineral.,* **86**, 1469–1476.

Robinson, P., Harrison, R.J., McEnroe, S.A. & Hargraves, R., 2002. Lamellar magnetism in the hematite-ilmenite series as an explanation for strong remanent magnetization, *Nature,* **418**, 517–520.

Robinson, P., Harrison, R.J., McEnroe, S.A. & Hargraves, R.B., 2004. Nature and origin of lamellar magnetism in the hematite-ilmenite series, *Am. Mineral.,* **89**, 725–747.

Rochette, P., 1987. Magnetic susceptibility of the rock matrix related to magnetic fabric studies, *J. Struct. Geol.,* **9**(8), 1015–1020.

Sato, A.M., González, P.D. & Llambías, E.J., 2003. Evolución del orógeno Famatiniano en la Sierra de San Luis: magmatismo de arco, deformación y metamorfismo de bajo a alto grado, *Revista de la Asociación Geológica Argentina,* **58**(4), 487–504.

Siegesmund, S., Steenken, A., López de Luchi, M.G., Wemmer, K., Hoffmann, A. & Mosch, S., 2003. The Las Chacras-Potrerillos batholith

(Pampean Ranges, Argentina): structural evidences, emplacement and timing of the intrusion, *Int. J. Earth Sci.,* **93**(1), 23–43.

Sims, J.P., Ireland, T.R., Camacho, A., Lyons, P., Pieters, P.E., Skirrow, R.G., Stuart-Smith, P.G. & Miró, R., 1998. U-Pb, Th-Pb and Ar-Ar geochronology from the southern Sierras Pampeanas, Argentina: implications for the Palaeozoic tectonic evolution of the western Gondwana margin, Vol. 142, pp. 259–281, in *The Proto-Andean Margin of GONDWANA,* eds Pankhurst, R.J. and Rapela, C.W.. Geological Society of London Special Publication.

Stuart-Smith, P.G., Camacho, A., Sims, J.P., Skirrow, R.G., Lyons, P., Pieters, P.E., Black, L.P. & Miró, R., 1999. Uranium-lead dating of felsic magmatic cycles in the southern Sierras Pampeanas, Argentina: implications for the tectonic development of the proto-Andean Gondwana margin, in *Laurentia-Gondwana Connections before PANGEA,* Vol. 336, pp. 87–114, eds Ramos, V.A. and Keppie, J.D.. Geological Society of America Special Paper.

Tarling, D.H. & Hrouda, F., 1993. *The Magnetic Anisotropy of Rocks,* Chapman & Hall, London, 217 pp.

Thompson, J.F.H., Sillitoe, R.H., Baker, T., Lang, J.R. & Mortensen, J.K., 1999. Intrusion-related gold deposits associated with tungsten-tin provinces, *Mineralium Deposita,* **34,** 323–334.

Whalen, J.B. & Chappell, B.W., 1988. Opaque mineralogy and mafic mineral chemistry of I- and S-type granites of the Lachlan fold belt, southeast Australia, *Am. Mineral.,* **73,** 281–296.

Zaccarini, F., Garuti, G., Ortiz-Suárez, A. & Carugno-Durán, A., 2004. The paragenesis of pyrophanite from Sierra de Comechingones, Córdoba, Argentina, *The Can. Mineral.,* **42,** 155–168.